Thickness-dependent selection of adhesive joints

Charline van Innis[1*], Thomas Pardoen[1,2]

[1]*Institute of Mechanics, Materials and Civil Engineering (iMMC), UCLouvain, Louvain-la-Neuve, Belgium*

[2]*Wel Research Institute, avenue Pasteur, 6, 1300 Wavre, Belgique*

*Corresponding author: Place Sainte Barbe, 2, 1340 Louvain-la-Neuve; charline.vaninnis@uclouvain.be

Thickness-dependent selection of adhesive joints

The fracture resistance of adhesive joints depends on the bondline thickness, especially in the toughest systems. While increasing the adhesive thickness to operate at peak fracture toughness is anticipated as attractive, it leads to a mass increase and to a decrease of the effective shear stiffness and strength, calling for a trade-off. Here, we follow a rational materials selection approach for mechanical design to address different sets of objectives and constraints representative of different classes of applications. The approach is applied to select the best conventional adhesive based on a novel database. Mechanical analysis with two different degrees of complexity is considered. The elementary level only accounts for the influence of thickness on toughness while more advanced models introduce the dependence of shear strength on thickness as well as the stiffness mismatch with the adherends. The best adhesive choice strongly depends on the objectives, constraints and loading configuration. However, the ranking is not drastically affected by the adherends stiffness. Gaps found for stiff/strong and tough adhesives motivate the development of architected joints. Inserting stop holes improves damage tolerance and density but reduces the shear strength and stiffness, requiring an optimum design.

Keywords: adhesive joint, materials selection, fracture toughness, strength, thickness, architected joints.

1. Introduction

The manufacturing of complex structures such as windmills, planes, marine hulls and cars involves a vast number of joints, that are usually made by welding, mechanical fastening, and/or adhesive bonding. Adhesive bonding permits the assembly of both similar and dissimilar materials leading to mass savings and to homogeneous stress transfer across the joint [1]. However, the design of adhesive joints is a complicated task due to the large number of variables to be controlled[2–5] making complex the development of robust failure assessment frameworks as requested by qualifying agencies.

The mechanical performances of adhesive joints depend upon the adhesive thickness *t* which influences the toughness, G_{Ic}, of the joint as well as the tensile strength, shear stiffness and shear strength. In general, the toughness increases with thickness until reaching a maximum at a thickness t^* corresponding approximately to the plane stress plastic zone size of the bulk adhesive equal to $2G_{Ic}E_a/(\pi\sigma_{0a}^2)$ where E_a and σ_{0a} are the adhesive Young's modulus and yield strength, respectively [6–8]. With increasing thickness, the degree of constraint in the bondline decreases, and the restriction on the development of the plastic zone is reduced. The degree of constraint is the highest for thin adhesive layers, leading to a high triaxial stress state ahead of the crack tip [9], which may lead to a change in failure mechanism [10, 11]. With increasing *t*, the plastic zone can expend into a larger volume and more energy can be dissipated by plastic deformation (Figure 1a). For large thicknesses, two different behaviors are reported. In some adhesive systems, once the maximum G_{Ic} is reached at $t = t^*$, the fracture toughness does not vary anymore with *t*, corresponding to adhesive A in Figure 1a [7, 12]. However, in other systems, after the optimum thickness has been attained, G_{Ic} decreases (adhesive B) as a result of the reduction of the plastic dissipation originating from shear stresses near the interface, to reach a lower plateau [6–8]. Note finally that in adhesive joints, K_{Ic} or G_{Ic} are usually not taken as the initiation fracture toughness, but as the steady state propagation value, knowing that the R-effect is usually weak or not observed at all [12–16].

Increasing the bondline thickness results in a reduction of the effective tensile and shear strength [17–21]. This is explained on the one hand by the fact that increasing *t* statistically leads to a larger number of larger microdefects (e.g. entrapped air) in the bondline [22] and, on the other hand, by the fact that when *t* increases, the stress state in the bondline varies and stresses tend to localize at the interface with the adherends near the joint edges (Figure 1b-c) [17, 19, 23] promoting adhesive instead of cohesive failure. This strength reduction is dependent upon the type of adhesive. Lap-shear tests have shown that this effect is less marked for ductile adhesives compared to brittle ones [21]. Finally, the stiffness also tends to decrease with increasing thickness [22]. Both stiffness and strength are influenced by the joint geometry and adherends material properties as these parameters influence the stress distribution in the bondline. The adhesive thickness must thus be considered when searching for the optimum design of reliable adhesive joints.

The systematic materials selection approach in mechanical design pioneered by M.F. Ashby[24] starts by translating a given application/function into objectives and constraints. Next, “performance indices” are derived, also sometime called “figures of merit” or simply “material indices”. These indices are usually combinations of material properties, sometimes associated to geometry or loading parameters in more complex cases. This translation into objectives and constraints is followed by the elimination of the materials that do not meet the hard design requirements. This results into a list of potential materials among which the best choice is the one that maximizes the performance index or a weighted function of at least two indices. In the simple selection problems, the performance index is a group of material properties decoupled from the loading and geometry, making the final selection relatively straightforward and only based on materials properties. However, when properties depend on a dimension, as addressed here, the problem gets more complex and often requires a more advanced modelling effort.

The goal of the present study is to apply, for the first time, the materials selection approach to adhesive joints while systematically considering the impact of the adhesive layer thickness. Although bringing extra degrees of complexity in the analysis, this choice to include thickness effects will prove the existence of some non-obvious trade off and selection options depending on the constraints and objectives. Furthermore, we will not only address conventional joints, but also architected solutions, enlarging the window of options as also proposed by Ashby in the extension of the selection procedure to hybrids [24, 25]. During the past ten years, researchers indeed developed architected joints by inserting meshes [26, 27], stop holes [27, 28], metamaterials [29, 30] in the bondline or by patterning the adherend surface [31, 32] to improve the joint toughness, but generally without comparing the solution to classical adhesive joints or without addressing other constraints in parallel.

The mechanical models used to describe representative joint loading configurations are introduced in section 2. Then, the selection method is detailed in section 3 and applied to several case studies, in section 4, for conventional joints, and, in section 5, for architected joints. The limitations of the analysis are discussed in section 6. In order to apply this methodology to real adhesive joints, a wide range of literature data has been collected. These data include the fracture toughness and variation with adhesive thickness as well as bulk adhesive Young's modulus, Poisson ratio, tensile strength and, when available, density, type of adherends, bonding process, resistance to chemicals, humidity and maximum service temperature. The database is contained in .csv and .txt files which are called by a MATLAB app performing the adhesive selection based on the loading conditions. This information is made open to the community (Supplementary Material).

2. Mechanical models of adhesive joints

This section presents the analytical or semi-analytical models that will be used to relate the critical load applied to a structural joint, schematized in a generic way in Figure 2, to the mechanical properties of the adhesive joint in terms of fracture toughness and strength, taking the thickness effects into account. Two different loading conditions will be addressed in order to cover a range of realistic configurations involved in adhesively bonded components: the *butt joint* configuration that involves loads predominantly normal to the plane of the joint and the *shear lap* configuration to treat conditions where the loading is a macroscopically applied shear. Depending on the degree of complexity and assumptions that are selected, the analysis can go quite far and is then often not amenable to analytical treatment. Among others, the stiffness of the adherends can affect the mechanics of the bondline [7, 33–35]. Now, the goal of the study is primarily to look at the optimum choice of adhesive including its thickness, and not at predicting the failure load exactly. The objective is thus to use models that produce the right dependencies on the parameters playing the primary role in setting the magnitude of the failure load (i.e. fracture toughness, strength, stiffness, thickness) so that the ranking of the adhesives will be correct. Two levels of modelling are addressed. A simplified level neglects the effect of the adherend stiffness as well as other advanced effects that influence the stress distribution in the bondline such as related for instance to the adherend thickness, the adherend rounding and/or tapering. This first level is interesting when comparing, for example, different solutions for architected adhesive joints as done in section 5.1. A more advanced level of modelling is then addressed to produce a more accurate description of the mechanics of adhesive joints under dominantly tensile or shear loading conditions relying on the literature [23, 36–38], as presented in sections 2.1.2 and 2.2.2.

2.1. Tensile butt joints

Tensile butt joints are often used to determine the tensile strength of an adhesive joint. Two large blocks made of the adherend materials, with Young's modulus E_s, are bonded with an adhesive layer of modulus E_a and thickness t as shown in Figure 2 with $L_{s1} = L_{s2} = L_a$. The joint contains a crack of length *2a* at its center, assuming that the only possible defects are voids developing during curing, treated as a crack, neglecting the fact that during in-service life, damage can also develop at the edges of the joint due to corner stress singularity. A damage tolerant approach is thus adopted to determine the joint tensile strength. The toughness G_{Ic} is thickness dependent, hence $G_{Ic} = G_{Ic}(t)$. The joint tensile strength is referred as the effective tensile strength σ^{f*} to be contrasted with the adhesive strength σ_a^f which would correspond to a material without major defects nor macro stress concentration (as measured in a clean uniaxial tensile test on bulk samples for instance). Experimentally, increasing *t* first leads to an increase of σ^{f*} [39, 40] which is followed by a decrease of σ^{f*}[17, 19, 39, 40] once *t* is larger than the optimum thickness. This decrease has two main origins. First, when increasing *t*, the stress state in the bondline and, more precisely, near "the corners" (where the interface meets the external surface), changes involving larger tensile stresses and sometimes a transition towards adhesive failure. Second, increasing *t* statistically leads to a larger defect density (e.g. entrapped air[22]). The adherends Young's modulus can also have an influence on σ^{f*} [36].

2.1.1. Simple model for pre-cracked butt joint

The influence of the adherends is neglected. Depending on the crack length, the failure of the joint[1], dictated by cracking of the adhesive, will be governed by either the bulk adhesive tensile strength σ_a^f or by the adhesive fracture toughness $G_{Ic}(t)$ or $K_{Ic}(t)$. K_{Ic} is related to the critical energy release rate G_{Ic} by $K_{Ic} = \sqrt{G_{Ic}E_a^*}$ where E_a^* is equal to E_a under plane stress conditions and equal to $E_a/(1-\nu_a^2)$ under plane strain conditions, and ν_a is the adhesive Poisson ratio. If the crack is short with respect to the joint dimensions, the adhesive strength governs failure and the effective tensile strength is bound by σ_a^f, hence:

$$\sigma^{f*} = \sigma_a^f. \tag{1}$$

For cracks longer than the critical crack length given by $a_c(t) = G_{Ic}(t)E_a^*/\pi\sigma_a^{f\,2}$, the resistance of the joint is set by the fracture toughness of the adhesive. To avoid failure, the remote stress intensity factor K^∞ must be lower than $K_{Ic}(t)$ of the adhesive leading to

$$\sigma^{f*} = \frac{K_{Ic}(t)}{Y\sqrt{\pi a}}, \tag{2}$$

where Y is a geometric factor equal to 1 if $2a \ll L$ and W. Eq. (2) is equivalent to

$$\sigma^{f*} = \frac{1}{Y}\sqrt{\frac{G_{Ic}(t)E_a}{\pi a(1-\nu_a^2)}}. \tag{3}$$

The transition from one regime to the other takes place at the critical crack length $a_c(t)$. Depending on the magnitude of $2a$, failure may be governed by the strength for some range of thickness and by the toughness for other thicknesses.

[1] The term "failure" means that at least macroscopic damage is initiated in the adhesive. Under some conditions, unstable crack propagation can take place leading to complete adhesive fracture while in other cases, the crack may start propagating without complete failure.

2.1.2. More advanced model for pre-cracked butt joint

The effect of adherend stiffness is now taken into account. Van Loock et al. [36] investigated the influence of crack length, fracture toughness and elastic modulus mismatch ratio on the adhesive tensile strength. A fracture process zone model was introduced through a traction separation law, characterized by a finite peak strength σ_{peak} set equal to σ_a^f [2] (while the second characteristic parameter of the law is related to G_{Ic} as the work of separation). The fracture process zone has a length l_s which sets an important length scale in the analysis. In the limit of very high σ_{peak}, one falls back onto a single parameter (G_{Ic}) problem for which the authors proposed a simplified analytical treatment[3]. Four regimes were evidenced by Van Loock et al. instead of two. The two first regimes (A and B in Figure 3) correspond to the short crack case for which the failure of the joint is only governed by the adhesive properties and for which

$$a + l_s(t) < 0.15t, \tag{4}$$

with the fracture process zone length l_s (for which thickness dependence is introduced here) given by

$$l_s(t) = \frac{E_a^* G_{Ic}(t)}{\pi {\sigma_a^f}^2}. \tag{5}$$

In regime A, joint failure is governed by the adhesive strength while in regime B, it is governed by the fracture toughness. Strength-controlled fracture takes place when

$$l_s > 3.37a, \tag{6}$$

and the effective tensile strength is obtained by solving

---

[2] This is an assumption that considers σ_a^f as the "intrinsic" strength of a bulk adhesive material with no defect, and disregards the crack tip constraint effect (e.g. [79]).

[3] When only considering the crack length with respect to the adhesive thickness, Van Loock et al. suggests as simplified analytical treatment $\sigma^{f*} = \sqrt{(E_a^* t)/(E_s 2\pi a)}$ which is valid for large σ_{peak}, falling back on one parameter despite of the fracture resistance.

$$\frac{2l_s}{t} = \frac{8}{\pi^2}\frac{2a}{t}\ln\left[sec\left(\frac{\pi\sigma^{f*}}{\sigma_a^f}\right)\right] . \quad (7)$$

For the two other regimes (C and D in Figure 3), one considers cracks of intermediate length as well as long cracks. The influence of the substrates can no longer be neglected, with a potential shielding effect on the crack. If it is assumed that both the adherends and the adhesive have the same Poisson ratio, the strength of the joint is obtained by solving

$$\frac{2l_s}{t} = \frac{8}{\pi^2}\frac{E_s^*}{E_a^*}\frac{2a}{t}\ln\left[sec\left(\frac{\pi\sigma^{f*}}{\sigma_a^f}\right)\right] + \frac{1-\bar{\nu}^2}{\pi}\left(\frac{\sigma^{f*}}{\sigma_a^f}\right)^2\left(1-\frac{E_s^*}{E_a^*}\right)\left(1-\frac{2a}{L_a}\right)^{-2} , \quad (8)$$

with $\bar{\nu} = \nu/(1-\nu)$ and L_a, the bonded length. The transition between the strength-governed regime D and the toughness-governed regime C is given by

$$\frac{2l_s}{t} = 3.37\frac{E_a^*}{E_s^*}\frac{2a}{t} + 0.31(1-\bar{\nu}^2)\left(1-\frac{E_a^*}{E_s^*}\right)\left(1-\frac{2a}{L_a}\right)^{-2} . \quad (9)$$

This analysis considers thus four non-dimensional parameters: a/t, l_s/t, E_a/E_s and a/L_a as shown in Figure 3. First, the transition between the short crack regime and the intermediate and long crack regime given by Eq. (4) is independent of E_a/E_s, as well as of σ^{f*} (Eq. (7)). In the intermediate and long crack regimes, the transition from regime C to D and the magnitude of σ^{f*} for given l_s and a depend on E_a/E_s. By decreasing E_a/E_s, the shielding effect of the stiff adherends is more pronounced, resulting in a larger σ^{f*} for given a, l_s and t.

The model derived by Van Loock et al.[36] does not consider the fact that, sometimes, when increasing the adhesive thickness, the joint tends to fail by adhesive failure or cohesive failure close to the interface, leading to a decrease of the effective tensile strength. This arises from the stress singularity at the interface corner. Reedy and Guess [23] derived a model based on an interface corner stress intensity factor to predict σ^{f*}, assuming that failure only takes place near the interface and that the joint is free from any defect. In tensile butt joints, the interface corner stress singularity order is $\lambda - 1$. Hence, the stress components near the corner can be expressed as $\sigma_{ij} = K_f r^{\lambda-1} f_{ij}$ with K_f the interface corner stress intensity factor and r the distance from the corner. For a semi-infinite layer of thickness t, the effective tensile strength is then given by

$$\sigma^{f*} = \frac{(1-\nu)}{\nu} \frac{K_f}{A_p(\nu)} \left(\frac{t}{2}\right)^{\lambda-1} \qquad (10)$$

where $A_p(\nu)$ and λ are derived in appendix A. A complete model must thus consider the presence of a crack, but also of the stress singularity at the interface corner.

2.2. Lap shear joints

The single lap-shear test is the most common test used by the industry to determine the joint shear strength. However, in single lap-shear, stresses do not uniformly develop in the bondline and the bending of the adherends lead to the development of peel stresses near the edges making the analysis difficult [34, 41]. Hence, it provides an "apparent" shear strength which is strongly dependent upon the adherend properties (Young's modulus and yield strength), adherend thickness, overlap length, and distance between the loading point and the bonded part. The shear strength is also influenced by the adhesive thickness due to the change in stress state in the bondline and the increasing presence of defects as t increases. Here, a thick adherend shear test (TAST) configuration is considered to avoid extra complexity associated to regular single lap-shear test. In addition, we neglect here the mode II fracture mechanics problem associated to the centered crack in the adhesive layer used for the case of butt tensile joints is neglected.

2.2.1. Simple mechanical description of shear lap configuration

For the elementary analysis, the geometrical parameters and adherend properties are neglected. Hence, it is simply assumed that failure occurs when

$$\tau^{f*} = \tau_a^f, \quad (11)$$

with τ_a^f being the "ideal" shear strength of the bulk adhesive as measured on as perfect as possible system. Eq. (11) has no influence of the thickness, leading to an overestimation of the effective shear strength.

2.2.2. Advanced model for shear lap configuration

For this second level of analysis, the effect of the adherend properties and of the thickness are now taken into account. Models outside fracture mechanics formalism have been derived in order to predict the lap-shear strength. However, these models fail to correctly capture the evolution of τ^{f*} with t, predicting an increase instead of a decrease as t is reduced [42]. Models based on finite fracture mechanics are more successful but require numerical simulations which would make the selection analysis cumbersome [43]. Some authors suggested to use a Generalized Stress Intensity Factor (GSIF) approach[37, 44–47] to predict the joint shear strength when adhesive failure occurs or cohesive failure takes place close to the interface. If we consider of lap-shear or TAST configuration, the presence of corners, see Figure 2 when $L_{s1}, L_{s2} > L_a$, at the joint edge induces a singular stress field. The order of the singularity is denoted as λ-1 and the magnitude of the stress field is scaled by the parameter H. Stresses at a distance x from the corner and in the direction given by the angle θ are then expressed as $\sigma_{ij}(x,\theta) = Hx^{\lambda-1}f_{ij}(\lambda,\theta)$. It was postulated that the joint failure occurred when H is equal to a critical value H_c. However, several studies have shown that H_c is both dependent on material properties and on the joint geometry. Regarding the joint geometry, increasing both the adhesive and the adherend thickness results in a decrease of H_c while increasing the overlap length and the free length (unbonded length between the loading point and the overlap) increases H_c[47]. In addition, a higher joint shear strength is not correlated with a higher H_c. An expression for H has been given by Askarinejad et al. [37]: $H = \tau^{\infty} t^{1-\lambda} b(\alpha, \beta)$ which depends both on material properties (λ, α, β) and on the joint geometry (t and b). More details on the determination of λ for the TAST configuration is given in Appendix B. Based on this GSIF approach, we heuristically assume that the effective shear strength is given by

$$\tau^{f*}(t) = \begin{cases} \tau_a^f & for\ t \leq 0.1 \text{ mm} \\ At^{\lambda-1} & for\ t > 0.1 \text{ mm} \end{cases}, \quad (12)$$

with A such that $\tau^{f*}(t = 0.1\, mm) = \tau_a^f$. The adhesive selection can be affected by this arbitrary choice, but its only purpose is to provide examples in section 4.1.2 when addressing the influence of t and E_s on τ^{f*}. Note that the power law variation will involve an exponent -0.35 (assuming λ = 0.65) for a corner not so far from the exponent -0.5 for a sharp crack under mode II. It is important to note that there exists an optimum thickness maximizing the joint shear strength, although it is not often reported in the literature[48]. Below this thickness, the shear strength tends to increase as t increases while any increase in thickness leads to a decrease in τ^{f*} at larger thicknesses as considered by Equation (12). This optimum thickness for instance depends on surface roughness. As this optimum thickness is dependent on several parameters and is often not reported, it has been decided to keep it as equal to 0.1 mm for all adhesives and the dependence of τ^{f*} below the optimum thickness is neglected by assuming a constant shear strength. This equation thus not necessarily predict the joint shear strength with high accuracy, but is sufficient to correctly rank the adhesives of the database by considering a decreasing strength as thickness increases and the elastic mismatch between the adhesive and adherends.

It is important to note that the GSIF approach has been developed for brittle adhesives and has been extrapolated to ductile adhesives in the present analysis. Using a brittle adhesive model for ductile adhesives can lead to an underestimate of the joint shear strength as ductile adhesives tend to be tougher and that an increase in toughness often results into an increase in joint shear strength[35]. Note also that we are not treating in this study the case of a lap-shear configuration with a pre-crack undergoing a complex mixed mode loading. We will discuss this limitation at the end of the paper.

2.3.Summary of the models

The different key equations of the models presented before that will be used next to describe the representative loading configurations are summarized in Table 1.

3. Adhesive selection methodology

The geometry shown in Figure 2 is considered. A shear force F_τ is applied parallel to the bondline and results in a transverse displacement u_τ while a normal force F_σ acts perpendicular to the bondline in which a crack of length *2a* is present. The joint width is *W*, the adhesive length L_a while the top adherend length is L_{s1} and the bottom adherend length L_{s2} with $L_{s1}, L_{s2} \geq L_a$ to generate both 180° and 90° corners. It refers thus to a situation combining a tensile load similar to that applied on tensile butt joints and a shear load corresponding to a TAST shear lap joint. As mentioned in sections 2.1.2 and 2.2.2, the corners lead to stress singularity (its order depends on E_a, E_s and corner angle) in the adhesive layer that can cause joint fracture. The impact of geometrical parameters such as the adherend's thickness and overlap length in lap-shear joints are thus omitted in order to limit complexity and focus on adhesive performances. For several applications, the adhesive thickness must remain within certain bounds set by a minimum thickness $t_{min} > 0$ µm and a maximum thickness t_{max}. This range must be considered during the selection procedure. It can either result from manufacturing constraints such as in windmills blades for tolerance or geometry reasons or by compactness requirements such as in laptops or appliances. Hence t_{min} and t_{max} enter as two extra parameters involved in the selection process. The Ashby selection approach starts with the statement of the objectives and constraints (step 1 in Figure 5).

3.1.Objectives

The objective(s) depend on the application and on the function of the joint in the application. Several objectives are contemplated to cover a variety of options. The two first objectives are classical for applications driven by a combination of economic and environmental concerns: (1) minimization of mass and/or (2) minimization of cost. The third objective (3) is the maximization of the fracture toughness. Recently, this objective motivated the design of tough joints through bondline architecturing, interface patterning and more generally through triggering additional toughening mechanisms[27, 49]. Directly linked to this objective, the fourth one (4) is the maximization of the tensile force that can be applied to the joint. Finally, in some applications focused on small dimensions, thickness minimization can also be an objective (5). The reasons that can push to one or a combination of these are addressed in what follows.

3.1.1. Mass minimization

For some applications, lightweight is required like in aeronautics or automotive to decrease fuel consumptions. However, adhesives must be tough, strong and stiff enough to comply with the structural constraints. As G_{Ic} increases with *t,* a trade-off must be found between a thicker adhesive and cost of a mass increase. For instance, the Aston Martin DBX contains 23 kg of adhesives [50]. If, for the sake of increasing toughness, the thickness is increased by 50%, the extra mass would be ~12 kg and the extra cost, assuming 100 euros/kg, would be > 1000 euros without taking into account additional fuel consumption costs. Another field where adhesive thickness is adding significant mass to the structure is in windmills blade. Adhesive thicknesses up to 30 mm are reported

[51]. Mass minimization can thus, in some cases, be a relevant objective (sometimes with a second objective). The mass of the structure is given by

$$m \equiv \rho_a L_a W t + \rho_s W h_s (L_{s1} + L_{s2}) \,, \tag{13}$$

where ρ_a and ρ_s are the adhesive and adherend's density, respectively. We assume that the nature and geometry of the adherends have been selected based on constraints put on the overall structure independent of the adhesive choice. Hence, one is left with minimization of the adhesive mass:

$$m \equiv m_a = \rho_a L_a W t \,. \tag{14}$$

3.1.2. Costs minimization

Cost comprises the cost per unit mass of the adhesive, but also the manufacturing cost:

$$C \equiv C_{adhesive} + C_{manufacturing} = C_a \rho_a L_a W t + (C_m t L_a W + C_{fixed}), \tag{15}$$

where C_a is the cost of adhesive per kg and the manufacturing cost involves both fixed costs C_{fixed} (molds, fixtures …) and variable costs which are related to the curing of the adhesive, C_m. When the costs are known, the analysis made for the mass can directly be used.

3.1.3. Maximization of fracture toughness of the joint

Knowing that a remnant bottleneck to the widespread use of structural adhesives is the real, or perceived, limited fracture toughness, one can consider as an objective per se. Recently, several research groups worked on adhesive toughening by triggering several dissipation or shielding mechanisms by playing with the joint architecture (see review in Chapter 33 of [49]). For example, Maloney and Fleck [27], Heide-Jorgensen and Budzik [28, 52] inserted holes in the bondline to blunt the crack tip to increase G_{Ic}. Others suggested to pattern the interface to induce mechanical interlocking and/or mode II components, at the microscale [53, 54] or at the macroscale [55–57]. Another toughening mechanism is crack bridging which can be triggered by playing on surface treatments [31] or by inserting meshes in the adhesive [55, 58]. The insertion of metamaterials within the bondline has been suggested [29, 30]. For this objective (3), the selection statement is “the best adhesive is the toughest one that meets all constraints for the considered range of adhesive thicknesses”.

3.1.4. Maximization of applied tensile force

An alternative to the maximization of G_{Ic} is the maximization of the remote tensile stress applied on the joint σ^{∞}. Compared to the previous objective, it considers or not the presence of cracks in the adhesive and the influence of the adherends on the selection. In this case, the selected adhesive is the one with the largest effective tensile strength σ^{f*} for a given crack length and range of adhesive thickness that meets the constraints.

3.1.5. Minimization of adhesive thickness

Several applications are constrained by compactness (in appliances, laptop, etc). In this case, the selected adhesive will be the one meeting all the constraints for the lowest possible thickness.

3.2. Constraints

Three constraints are envisioned:

a. The joint must support a prescribed tensile force without failure.
b. The joint must support a prescribed shear force without failure.
c. The joint must exhibit a prescribed level of shear stiffness (this is equivalent to stating that the shear displacement under the prescribed shear force cannot be larger than a threshold value, e.g. for dimensional tolerance).

These constraints can be combined or not. In real applications other constraints must of course be imposed in terms of resistance to fluids, thermal degradation, or fatigue which will be addressed in future extensions of the present study. The three constraints are now connected to the mechanical models presented in section 2. Finally, one can see the crack length *a* also as a geometric constraint.

3.2.1. *Tensile loading constraint*

The first constraint is to resist the tensile force F_σ, resulting in a remote applied tensile stress $\sigma^\infty = F_\sigma / L_a W$. Depending on the level of analysis, either Equations 1 to 3 or Equations 4 to 9 are considered. Hence, failure is assumed to occur by a cohesive mechanism only (e.g. fracture inside the adhesive) as it originates from the centered crack lying in the middle of the adhesive layer. The joints are assumed free from any other defect than the pre-existing crack of length *2a*. Stress singularity at the joint edge due to material mismatch, as considered by Eq. 10, is thus neglected in what follows. Generally speaking, σ^∞ must remain lower or equal to the effective tensile strength of the joint as stated by

$$\sigma^\infty \leq \sigma^{f*}. \tag{16}$$

Depending on the model, the analysis changes as explained in section 2.1. In the elementary approach, σ^{f*} is given by Eq. 1 or 3 depending on the crack length. In the more advanced description, the interactions between the adherends and adhesive are considered. In this last case, if the fracture toughness and the crack length are such that Eq. 4 is satisfied, σ^{f*} is equal to σ_a^f if Eq. 6 is satisfied and if not, it is given by solving Eq. 7. If Eq. 4 is not satisfied, Eq. 8 is used to determine σ^{f*}.

3.2.2. *Shear loading related constraints*

The second constraint is related to the shear load, F_τ, resulting in a mean shear stress $\tau^\infty = F_\tau / LW$ in the bondline and in an overall longitudinal displacement u_τ. This displacement cannot exceed a maximum value u_τ^{max}, set by the minimum shear stiffness admissible for the component. Under a pure shear load, the shear stiffness is governed by the adhesive. The shear stiffness is expressed by

$$\frac{\tau^\infty}{u_\tau^{max}} < \frac{\mu_a}{t}, \tag{17}$$

where μ_a is the adhesive shear modulus. This assumption gives an upper limit for the joint shear stiffness which corresponds to cases for which the adherends are stiff and/or thick [59, 60]. In addition, F_τ must not induce any shear failure so that the shear strength τ^f, of the joint which is dependent upon *t*, cannot be exceeded:

$$\tau^f \leq \tau^{f*}. \tag{18}$$

With the elementary model, the change in stress state in the bondline as *t* increases is not considered and it is assumed that τ^{f*} is constant and equal to the bulk adhesive shear strength approximated by

$$\tau^{f*} = \frac{\sigma_a^f}{\sqrt{3}} . \tag{19}$$

In the advanced description, the influence of the thickness and the adherends' elastic properties is considered through Eq. 12.

3.3. Selection scenarios

Depending on the considered set of objective(s) and constraints (as emerging from different types of structural applications), several selection scenarios are possible. One can contemplate a single objective and a single constraint resulting in a method similar to the most basic approach, see also [24]. However, it is also possible to consider several objectives with one or more constraints. Here, for the sake of illustrating the approach and revealing several interesting non-trivial, trade-off problems with only one objective but with several constraints will be addressed:

- Scenario 1: Mass minimization with constraint on tensile force, shear force and shear stiffness;
- Scenario 2: Cost minimization with constraints on tensile force, shear force and shear stiffness;
- Scenario 3: Fracture toughness maximization with constraints on shear force and shear stiffness;
- Scenario 4: Tensile stress maximization with constraints on shear force and stiffness;
- Scenario 5: Thickness minimizations with constraints on tensile and shear forces and shear stiffness.

This leads to different objective functions and, depending on the scenario, the objective function is combined or not with the constraints. If not, the constraints will correspond to a limit which will be translated into a possible range of thickness that can be selected. The analysis can be directly extended to several objectives[24] requiring then the introduction of weights to balance the impact of each objective on the optimization function.

The logic of the selection is schematically explained in Figure 4. The considered constraints will lead, for each adhesive, to a range of thickness inside which the adhesive can be selected as G_{Ic}, τ^{f*} and the shear stiffness all depend upon *t*. As G_{Ic} increases with *t*, the constraint will lead to a minimum thickness that can be selected (Figure 4a') to avoid failure. If the dependence of G_{Ic} is similar to that of adhesive B in Figure 2, it can also lead to a maximum thickness (Figure 4a''). At the opposite, as the effective shear strength and stiffness decrease with *t*, these two constraints result in setting a maximum thickness that can be selected (Figure 4b and c). The combination of the three constraints sets an acceptable thickness range inside which one can select the best thickness with respect to the objective function (Figure 4e) and this for each adhesive; and of course, if the constraints are too severe, some adhesives will end up never meeting these whatever the thickness. The best adhesive (chosen at its optimum thickness) is the one that maximizes or minimizes the objective.

If the constraints do not enter the objective function as for scenarios 3 to 5, the selection will be made based on the constrained thickness range, as long as it is comprised in the range between t_{min} and t_{max}. Maximizing the fracture toughness is thus similar to selecting the adhesive characterized by the largest fracture toughness in the acceptable regime of thicknesses. When the tensile force is maximized, failure is governed either by the strength or by the fracture toughness, the selection is now dependent on the crack length. In this case, for a given crack length, the adhesive characterized by the largest effective tensile strength is considered. Finally, if the thickness must be minimized, the adhesive which can be selected with the lowest possible thickness is chosen. In this case, it is possible to have several adhesives that can be selected and that meet the mechanical requirements.

For scenario 1 and 2, depending on the constraints, a range of thickness will be determined for each adhesive, but the objective function is also dependent upon the constraints. Hence, the objective functions must be derived, requiring to isolate $L_a W$ in the constraint equations to be replaced then into Eq. (14) when minimizing mass and into Eq. (15) when minimizing cost. Only the objective function for the scenario 1 will be derived. Indeed, adhesive suppliers do not always make their price publicly available and the manufacturing cost is often unknown. Hence, it is difficult to give practical examples for this scenario. Nevertheless, the methodology is exactly similar to that of mass minimization. Regarding the derivation of the objective functions, one objective function is derived for each constraint. Regarding the tensile force constraint, the objective function, m_{TC}, is given by

$$m_{TC} = \frac{\rho_a t}{\sigma^{f*}} \, . \tag{20}$$

The shear stiffness constraint leads to Eq. (21) (objective function denoted as m_{sc1}) while the objective function corresponding to the shear force constraint, denoted as m_{sc2}, is given by Eq. (22).

$$m_{SC1} = \frac{\rho_a t^2 F_\tau}{\mu_a u_\tau^{max}} \, , \tag{21}$$

$$m_{SC2} = \frac{\rho_a t F_\tau}{\tau^f(t)} \, . \tag{22}$$

For each adhesive that meets the constraints, m_{TC}, m_{SC1} and m_{SC2} are computed. If at least two adhesives minimize the total mass, the adhesive characterized by the lowest maximum between m_{TC}, m_{SC1} and m_{SC2} is selected.

It is also important to note that when tensile and shear stresses are jointly applied to the joint, a combined failure criterion should ideally be used. Several failure criteria have already been developed such as a maximum stress or strain over a certain distance, an energy criterion, a global yielding criterion or a criterion based on failure envelopes [61–63]. Here, it has been decided to not apply here a combined failure criterion in order to not further complexify the model and because of the absence of relevant data on most of the considered adhesive systems. Hence, limits for tensile and peel stresses are evaluated separately. Except in the case of pure shear or tensile loading, this assumption leads to an overestimation of the maximum tensile and shear stresses that can be applied to the joint. The implementation of an interactive failure criterion is left for further deployment of the methodology, although one does not expect significant changes in the final rankings.

The assumptions mentioned previously regarding the geometry and the parameters having an influence on the joint shear and tensile strengths and on the shear stiffness are summarized here-below:

- Only two macroscopic loads are considered: tensile and shear loads; macroscopic peel is neglected.
- Assumptions regarding the tensile loading condition:
    - A through-thickness, centered crack of length 2*a* is assumed in the adhesive layer.
    - Failure is assumed to be cohesive only as it originates from the centered crack and not from a stress singularity caused by material mismatch and due to the presence of a corner at the joint edges (Equation 10 is not considered).
    - With the simple model, the influence of the adherends Young's modulus and of the crack length with respect to the adhesive thickness is neglected.
- Assumptions regarding the shear loading condition:
    - The presence of the centered crack is neglected due to the lack of data for mode II fracture toughness variations with thickness.
    - With the simple model, the joint shear strength is equal to the adhesive shear strength.
    - Advanced model: failure originates from the stress singularity due to the presence of the corner at the overlap edges. Failure is thus assumed to be cohesive near the interface.
    - Advanced model: the model has been developed for brittle adhesives, but it is also applied to ductile adhesives in the following examples.
    - Shear stiffness: the influence of the adherends Young's modulus and thickness is neglected while the thinner and the more flexible the adherends, the lower the shear stiffness [59, 60].

- Assumption regarding the combination of the shear and tensile loads: no interactive failure criterion is used and the limits for both loading conditions are assessed separately.

3.4. Database

Literature data regarding the influence of the thickness on adhesive joint properties have been collected from different sources, as reported in Table 2. However, when data were found for the fracture toughness, most often no data were given for the evolution of the shear strength with thickness. The opposite is also true. Consequently, literature data do not allow estimating the influence of thickness on fracture toughness and shear strength simultaneously. For the fracture toughness data, tests are usually performed only for a few adhesive thicknesses. Hence, for each adhesive, the data have been extrapolated to consider a broader range of thickness and extend the window of investigation (see Figure 5 step 3). Experimental data are fitted using piecewise cubic hermite interpolating polynomial (PCHIP). For thickness larger than the maximum available one, G_{Ic} is considered to be constant, equal to the last experimental data point. For thicknesses smaller than the available range, the two first data are considered and linearly extrapolated. This is done for each adhesive independently of the others. Finally, the tensile strength and the shear modulus are set to the bulk adhesive values. There is thus much room left for extending and refining the database in the future.

In addition to these constraints linked to the mechanical loading, constraints regarding the process conditions, the adherend materials (metal or polymer-based) and the operating environment can be introduced. Similar to the software EduPack [64], the constraints can be applied through checkboxes in the developed app.

Finally, the fact that thickness influences the adhesive properties does not lead to readable charts similar to those one found in Ashby's book [24]. Hence, in the present case, the selection graph (in the app) shows the effective tensile strength of the joint as a function of the thickness with the allowed thickness range corresponding to the green part of the graph in Figure 4d.

The selection procedure can be divided into 4 steps, schematized in Figure 5. The first step is the definition of the objective(s) and of the constraint(s) (see sections 3.1 and 3.2), then performance indices and objective functions are derived (see section 3.3). Then, the adhesive database is screened involving the extrapolation of the experimental data to determine for which range of thickness each adhesive meets the requirements (see section 3.4). Finally, based on the objective and on the derived indices, the adhesives are ranked to select the best one and its corresponding thickness.

4. Case studies for classical adhesive joints

Several scenarios are investigated and applied to mostly commercial adhesives for which reliable data regarding the evolution of the fracture toughness with t can be found in the literature, see section 3.4 and Table 2. For the sake of illustration, we describe in details the first scenario to minimize mass, and give in Appendix C and D examples for the maximization of K_{Ic} and σ^{∞}.The first scenario is to minimize mass. But, first, Figure 6 shows the Ashby maps giving $K_{Ic}(t \geq 0.2\ mm)$ versus (a) the adhesive tensile strength and (b) the Young's modulus for all the adhesives of the database. As a general trend, increasing the K_{Ic} is associated to a decrease of the adhesive Young's modulus while no obvious trend is observed regarding the tensile strength.

4.1.Mass minimization: elementary model

When minimizing mass, three constraints are considered: to support the applied shear and tensile forces and to meet a prescribed shear stiffness. This leads to a selection involving 6 parameters: $2a$, σ^{∞}, τ^{∞}, u_{τ}^{max}, t_{min} and t_{max}. First, the constraints on the tensile and shear loading are considered separately before analyzing their combined effect using here the elementary model. For all analyses, t_{min} is set to 200 µm simply because G_{Ic} data are not available for all adhesives[4] below this thickness.

4.1.1. Impact of the applied tensile load on the selection

Figure 7 addresses the influence of the remote tensile stress σ^{∞}, as well as the effect of crack length *2a* without any applied shear load τ^{∞}(=0). For each crack length, the remote tensile stress is varied, so that for each combination of σ^{∞} and $2a$, the lightest joint meeting the requirements is selected. In some cases, several adhesives meet the constraints and lead to joints of similar mass. In this case, the one with the lowest m_{TC} (Eq. 20) is selected, corresponding to the largest σ^{f*}. In addition, the failure regime (strength or toughness-dominated) is highlighted for each selected adhesive in Figure 7.

Depending on the magnitude of *2a,* σ^{f*} varies with the adhesive strength or with the fracture toughness. Zones corresponding to strength and toughness-governed regimes alternate in Figure 7 and the transition from one adhesive to the other occurs at a crack length such that $2a = 2a_c$. For very short cracks, the failure of all adhesives is governed by strength, leading to the selection of the strongest adhesive, i.e. BP907. With increasing

---

[4] This limit is set to ensure that the influence of *t* on G_{Ic} corresponds to the two types of influences shown in Figure 1 to not consider the fact that at very small thickness, a slight increase of G_{Ic} when decreasing *t* has been sometime reported due to the change of failure mechanism from propagation at the center of the bondline to propagation near the interface and failure by shear yielding [10, 80, 81].

crack length, failure of BP907 starts to be dominated by fracture toughness although it remains the strongest adhesive for $t = t_{min}$ as shown in Figure 7c. Further increasing *2a* leads to the selection of ESP110 which appears to be the strongest one at $2a = 1$ mm for $t = t_{min}$ (Figure 7d). As the crack length is progressively increased, it exceeds $2a_c$ for all adhesives. Hence, for large crack lengths, failure is dominated by fracture toughness only and the selected adhesive is the one characterized by the largest K_{Ic} for $t = t_{min}$ which is the adhesive F185. This first analysis already shows that the selection of the best adhesive significantly varies with the assumed/known crack size.

The magnitude of the applied tensile load plays a minor role in the selection compared to the crack length. For a given crack length, one indeed rarely sees in Figure 7 that the choice of the adhesive changes when changing the applied stress except for some small ranges of crack lengths (gray zones). These correspond only to conditions for which the adhesive minimizing the mass meets the requirements for a thickness larger than t_{min}. This is highlighted in Figure 7e where the maximum σ^{f*} for $t = t_{min}$ is equal to 25 MPa. However, some adhesives can carry larger stresses at larger *t*. For instance, if σ^{∞} is equal to 30 MPa (gray dashed line), the lightest joint meeting the requirements is with Betamate 1493 at *t*= 0.4 mm. This means that the selected adhesive is the one able to carry σ^{∞} for the lowest possible thickness in order to generate the lightest joint.

4.1.2. Impact of the applied shear load on the selection

The influence of the applied shear stress τ^{∞} and of the shear stiffness $\tau^{\infty}/u_{\tau}^{max}$ is shown in Figure 8 when imposing minimum adhesive thickness and applied tensile stress to 0.2 mm and 0 MPa, respectively. The shear strength dominates for low imposed stiffness and high applied shear load resulting in the selection of BP907, the strongest adhesive. Stiffness dominates the selection when high shear stiffness is required leading to the selection of Betamate 73455, the stiffest adhesive. For intermediate cases, the adhesive offering the best combination of strength and stiffness is selected which is here ESP110.

4.1.3. Combined applied tensile and shear loads

The simultaneous influence of the four parameters - *2a*, σ^{∞}, τ^{∞}, u_{τ}^{max} - is investigated based on the selection charts in Figure 9 which depend on *2a* and τ^{∞}. In Figure 9a, the shear stiffness and the remote tensile stress are set equal to 1000 MPa/mm and 5 MPa, respectively. The selection depends significantly on *2a* and τ^{∞}. For small crack lengths, the selection is dominated by stiffness for low values of τ^{∞} while the shear stress constraint dominates for large τ^{∞}. For large crack lengths, whatever the magnitude of τ^{∞}, the tensile constraint dominates, pointing towards the selection of the toughest adhesive. In between, there exists a zone where the shear stress and tensile constraints compete. For a given shear stress, increasing the crack length leads to a dominant tensile constraint instead of a dominant shear stress constraint. For a given *2a*, the shear stress constraint tends to dominate if τ^{∞} is increased.

The influence of σ^{∞} is investigated by comparing Figures 9a and 9b for σ^{∞} equal to 5 and 20 MPa. The maximum allowed crack length decreases as σ^{∞} increases. In addition, the zones over which the strongest adhesive is selected is reduced, highlighting the fact that, in this case, tensile load dominates over the shear load.

The influence of the shear stiffness is investigated in Figure 9a (1000 MPa/mm), 9c (100 MPa/mm) and 9d (10000 MPa/mm). For a low stiffness (9c), the selection is dominated by the shear and tensile constraints only. At large stiffness (9d), stiffness dominates the selection. As a stiffer adhesive tends to be more brittle, long cracks and high tensile stresses are not allowed for these joints indicating a gap in the available performances of current adhesives (more details in section 4.4). At intermediate stiffness (9a), the three constraints compete.

4.1.4. Influence of t_{min} and t_{max}

As the fracture toughness varies with the adhesive thickness, the choice of t_{min} and t_{max} affects the selection of the best adhesive. Considering a tensile load only (Figure 10a), if t_{min} is set to 5 mm (a quite large value as used sometimes for geometrical tolerance reasons in ship building or windmills – although much thicker joints exist up to 30 mm or higher [51]) for instance, at large crack length, SikaPower 498 is selected while when set to 200 µm, F185 is preferred. This arises because the G_{Ic}, and consequently σ^{f*}, of the SikaPower 498 is larger than that of F185 if $t_{min} > 0.6$ mm (Figure 7e,). If now t_{max} is varied and is lower than t^{*}, for a given crack length, the maximum tensile stress that can be applied, considering all adhesives of the database, is reduced, limiting the domain in which an adhesive can meet the constraint. Regarding, the shear stress and stiffness constraints only, decreasing t_{min} increases the maximum shear stress that can be reached while increasing it has the opposite effect. Hence, if t_{min} is increased, the softest adhesives will tend to no longer be selected, as shown in Figure 10b-d. When, the three constraints are combined, increasing t_{min} leads to a selection that is more and more dominated by the shear stiffness constraint, leading to the selection of more brittle adhesives. These effects arise from the dependence of G_{Ic} on t and due to the fact that tough adhesives tend to be flexible while stiff adhesives tend to be more brittle as shown in Figure 6.

4.2. Mass minimization: effect of adherend-adhesive stiffness mismatch

4.2.1. Tensile load

The results of Figure 11 are obtained taking into account the adherend-adhesive interaction based on the more advanced analysis of Van Loock et al. [36] and Askarinejad et al. [37]. A first key difference that emerges when compared to Figure 7 produced with the elementary level, is that adhesives can now be selected (and thus meet the imposed constraint) for larger crack lengths. Indeed, if $E_s = 200$ GPa, BP907 is selected up to a crack length of 70 mm instead of 0.5 mm. When the adherends Young's modulus is lower, the crack length for which one adhesive can be selected decreases as the shielding effect is reduced. Indeed, for E_s equal to 200, 100 and 10 GPa, the maximum $2a$ for which BP907 can be selected is equal to 70, 20 and 2 mm, respectively. In addition, compared to Figure 7, the selected adhesives are no longer the same. Indeed, ESP110 is no longer dominant and instead of selecting F185, FM1000 is now preferred. Indeed, F185 is two times stiffer than FM1000 but is characterized by a process zone of similar length. Van Loock et al. showed that if two adhesives of same σ_a^f and l_s are considered, the selected adhesive for given l_s/h and a/h will be the less stiff. For this reason, FM1000 is selected instead of F185 because, as shown in Figure 6, these are characterized by similar σ_a^f and K_{Ic}, but FM100 is the most compliant.

4.2.2. Shear constraints only

Figure 12 shows the influence of the imposed shear load and stiffness constraints on the selection if E_s is equal to 200 GPa. The selection is not drastically modified compared to the case where the interactions with the adherends are neglected. The strongest adhesive is still selected when a high shear load is applied while the stiffest one is selected when a high shear stiffness is imposed. When varying E_s to 10 GPa or 100 GPa, no difference was observed in the selection, except when increasing E_s, then the maximum shear strength that can be met slightly increases as λ in Eq. (B1) increases. In addition, the thickness effect is now introduced, leading to a lower maximum shear stress that can be carried when comparing Figure 12 to Figure 8.

4.2.3. Combined effects

Figure 13 shows selection maps for varying crack length and applied shear load, for different values of E_s and imposed shear stiffness. By increasing the adherends stiffness, the maximum shear strength and the maximum crack length for which an adhesive can be selected increase due to more pronounced shielding. In addition, increasing the adherend Young's modulus results in a selection more dominated by the applied shear load than by the tensile load.

4.2.4. Comparison with the elementary model

Regarding the tensile constraint, a simple "adherend independent" model leads to the selection of the adhesive with the largest K_{Ic} while the advanced analysis indicates a competition between the adhesive toughness and the shielding effect of the adherends that can lead to the selection of a slightly more brittle adhesive but softer. In any case, the simple approach captures the main trends which is to select tougher adhesives as *2a* increases and stiffer and stronger adhesive when the imposed shear load and stiffness increase.

4.3. Other objectives

The same procedure has been followed for the maximization of K_{Ic} or the maximization of σ^{∞}. The detailed results are shown in Appendix C and D. In both cases, the selection is strongly dependent on the constraints imposed for the shear load and stiffness. Increasing the magnitude of these constraints results in the selection of stiffer and stronger adhesives that are characterized by a lower fracture toughness. The main difference between these two cases, is the dependence of the selection on the crack length when maximizing σ^{∞} while maximizing K_{Ic} results in a selection independent on the crack length. When maximizing σ^{∞}, the maximum tensile force that can be carried by the joints decreases as the crack length increases. As for mass minimization, t_{min} and t_{max} also influence the selection due to the dependence of G_{Ic} on the adhesive thickness.

4.4. Gaps in adhesive property charts

Depending on the application and selection problem, gaps appear in the selection chart of adhesives as schematically drawn in Figure 14. This schematic chart represents in 3D the different constraints and the domain that can be met with existing adhesives. As shown previously, these gaps depend on thickness. For low t (t_1 in Figure 14), adhesive joints are generally characterized by high shear strength and stiffness, but lower fracture toughness. This leads to the definition of two gaps corresponding (1) to stiff and tough adhesives region and (2) to tough adhesives with high shear strength region. For high t (t_2 in Figure 14), the fracture toughness increases, but the shear strength and shear stiffness tend to decrease. Hence, here, three gaps are revealed: (1) high shear strength and stiffness region; (2) high shear strength and high toughness region; (3) stiff and tough region.

These gaps in the selection of adhesive materials have two origins: the adhesive thickness and the adhesive material. The influence of thickness has already been discussed. In addition to this, adhesives are characterized by antagonist performances "stiff, strong and brittle" and "soft, flexible and tough" as also shown in Figure 6.

Applications requiring high shear strength and stiffness will preferentially end up with thin adhesive bondlines, limiting the fracture toughness of the joint while thick-adhesive joints are better suited for applications with high fracture toughness, but allowing for limited shear stiffness and strength.

5. Case studies for architected joints

Bondline architecturing is one of the strategies that has been recently investigated by different research groups to increase the joint fracture toughness [27–30, 49, 65]. The question here is to assess if the potential of such solutions to indeed push the envelope of the selection leads to more optimal solutions compared to traditional joints taking into account the fact that other constraints play a role. The joint architecture can involve the addition of a mesh, stop holes or more complex metamaterials. Covering all possibilities goes beyond the scope of this work. Here, to illustrate the interest of the selection approach, one considers architected joints made of stop holes having a length *D*. *D* is determined based on the process zone length l_p [5]which is equal to $l_p = 1/\lambda_w$ [28]. λ_w is the elastic foundation wave number given by

$$\lambda_w = \sqrt[4]{\frac{m}{4}\frac{E_a}{t}\frac{W}{E_s I}} \quad \text{with} \quad m = \frac{1-\nu_a}{(1-2\nu_a)(1+\nu_a)}, \tag{23}$$

where I is the second inertia moment equal to $Wh_s/12$. It is thus dependent on the adhesive and adherend Young's moduli E_a, E_s and on the geometric parameters t, W, h_s. In the present case, 3D plane strain was assumed to derive the expression of *m*, a

[5] The process zone denoted by l_p is different from the l_s process zone. The l_p process zone refers to the length corresponding to the zone that extends from the crack tip to the zone where no deformations take place in the adhesive and the DCB arms. For more information, the reader is referred to [82].

parameter depending on the crack tip stress/strain state. Heide-Jørgensen and Budzik[28] showed that the joint fracture toughness is maximized when D is about $2l_p$.

In order to apply the materials selection approach to this class of architected joints, the maximum principal stress criterion developed by Martiny et al. [16] for the adhesive Betamate 73455 is implemented in Abaqus. Both Double Cantilever Beam (DCB) and lap shear joints are modeled to investigate the influence of the stop holes and of the adhesive thickness on the joint properties. More details are given in Appendix E. The height of the cavities is set equal to the adhesive thickness while their spacing is set to $2l_p, 4l_p$ and $6l_p$, leading to joints made of 50%, 33% and 25% of cavities. The spacing is known to not influence the fracture toughness if it is large enough [27]. However, they did not investigate the impact of the holes on the adhesive shear stiffness and strength. One anticipates that the shear stiffness decreases by increasing the number of cavities, and by decreasing their spacing, affecting then directly the selection of best solution depending on the problem. G_{Ic} and shear stiffness are computed for the different stop holes distributions using FE simulations. The shear and tensile strength are roughly estimated as given by

$$\sigma_{archi}^{f} = \frac{S - S_{holes}}{S} \sigma_a^f \quad , \tag{24}$$

$$\tau_{archi}^{f} = \frac{S - S_{holes}}{S} \tau_a^f \quad , \tag{25}$$

where σ_a^f and τ_a^f are the bulk tensile and shear strength of the plain adhesive. S is the real surface area of the joint, equal to $L_a W$, while S_{holes} correspond to the surface area occupied by the stop holes when orthogonally projected. $S - S_{holes}$ is thus the effective area covered by the adhesive over which the forces act. More advanced models for the strength of architected joints is left for future investigation, but one can already foresee that in stiffness and strength dominated problems, an architected joint will not outperform the traditional joints.

5.1.Objective on mass minimization

Four joints are considered, all made of the adhesive Betamate 73455 and 0%, 25%, 33% and 50% stop holes. The goal is to determine under which conditions an architected joint must be preferred to its classical counterpart.

5.1.1. Tensile dominated loading

The influence of σ^{∞} and *2a* on the adhesive selection is shown in Figure 15. The range of forces and crack lengths for which an adhesive with stop holes can be selected is modified compared to the plain adhesive joints considered before. The architected joint is associated to a larger effective tensile strength for long cracks. However, this depends on the amount of stop holes inserted in the bondline. Indeed, as shown in Figure 15b and c, the more the stop holes in the bondline, the lower the σ^{f*} as the effective cross-section area over which the tensile force acts decreases. Conversely, a reduction of the number of stop holes decreases the number of crack arrestors. In the current analysis, the crack tip is assumed to correspond to a stop hole. However, if the crack tip does not correspond to a stop hole, the toughness is first equal to the plain adhesive joint G_{Ic} [27] and when the crack reaches the next stop hole, the toughness is the one of the architected joint. The considered crack length is equal to $\max(2a, nD)$ with n being an integer and $n \geq 1$. The joint must be made of less than 33 % of cavities to improve the damage tolerance (Figure 15c). For small cracks, when the imposed tensile load increases, the selection points towards an adhesive with the lowest number of cavities as it corresponds to the joint with the larger effective cross-section area. Previously, the adhesive with the highest σ^{f*} was selected while in the present case it is no longer true because the weight saving coming from the introduction of holes dominates the selection for an objective based on mass minimization.

5.1.2. Shear loading

The joint with the largest proportion of cavities is always selected as long as its shear stiffness and strength are not exceeded as shown in Figure 16. Further increasing the imposed shear stress and stiffness leads to the selection of a joint with a lower amount of stop holes, until the plain adhesive joint remains the only one that can be selected. Indeed, decreasing the number of cavities in the bondline improves the shear strength and stiffness. When considering only classical adhesive joints, regions where the shear strength or stiffness dominate are both predicted, while here it is no longer the case because the lightweight of the architected joint dominates. When using an architected joint with stop holes, the required shear stiffness and strength are limited to lower values compared to conventional joints. Hence, inserting stop holes limits the joint shear properties.

5.1.3. Combined effects

The combined effects of $2a$, τ^{∞} and $\tau^{\infty}/u_{\tau}^{max}$ are investigated. No novel conclusion emerges compared to the former analysis. The damage tolerance is improved only if the required level of shear strength and stiffness remains moderate. Indeed, if the constraints on shear stress and stiffness are too large, a plain adhesive joint is preferred. Another advantage of architected joints is the associated weight saving owing to the presence of the cavities which act positively on density and toughness. This weight saving dominates the selection and not the tensile and shear constraints as for classical adhesive joints.

5.2. Other objectives

As for the classical adhesive joints, two other objectives have been applied to the selection of architected joints: K_{Ic} maximization (Appendix C) and maximization of applied load σ^{∞} (Appendix D). Compared to the mass minimization objective, when an architected joint can be selected among other architected joints with stop holes, in these two cases, it is the one containing the less stop holes. This arises from the fact that by increasing the amount of stop holes in the bondline, the effective cross section area over which the tensile and shear forces act decreases resulting in lower effective tensile strength, shear strength and shear stiffness. These two examples show that there is thus a trade-off to find when designing architected joints between the gain in fracture toughness and the loss in shear strength and stiffness and that the optimal design depends on the objective.

5.3. Filling gaps in adhesive property space

Introducing stop holes leads to an increase of the fracture toughness, but reduces the strength and stiffness. Hence, gaps left when considering classical adhesive joints are partly filled owing to architecturing (Figure 17). The spacing between the stop holes offers some degree of freedom to fill in this domain. In addition to toughening, bondline architecturing with stop holes results in lighter joints. But, for applications requiring high shear strength and stiffness, joints with stop holes may not be suitable. Bondline architecturing with stop holes is thus interesting for applications requiring low weight and high fracture toughness, but moderate strength and stiffness.

6. Limitations of the adhesive selection analysis

The selection analysis of the best adhesive system setup in this study although addressing many aspects, in particular with the incorporation of adhesive thickness effects, is still missing several elements while also relying on a few restrictive assumptions. Once again, the goal in a materials selection analysis is not to predict the exact failure load or exact joint performance, but to use models that are sufficiently correct to lead to the right ranking among different adhesives. In a few cases, an advanced model is required to avoid missing some effects, such as the adherend stiffness mismatch that may modify the selection; while in several other instances, the selection with an elementary model is appropriate. We review here the main limitations of the current study, aimed at paving the road for future works.

First of all, the database that has been compiled for the purpose of this study is incomplete both in terms of adhesive systems and in terms of specific data. There is a need to find and/or generate more extensive data on thickness effects on strength and toughness. Also, novel systems may exist or will emerge that will modify the conclusion made regarding best adhesive choice. These conclusions should thus be seen as illustrative and not definitive.

Then, although the database already accounts for other properties when available such as the temperature resistance, the resistance to humidity and the chemical and bonding processes, these have not been addressed in the present selection analysis. Many of these constraints, depending on the type of application, can be easily introduced simply through a "go – no go / yes - no" choice (already implemented in the MATLAB application).

Another key remnant issue in adhesive bonding is the importance of the surface treatment. Depending on the adherends and the adhesive, there exists an optimum roughness [66, 67]. Failure can be either cohesive or adhesive [68], affecting very much the strength of the joint. For example, in peel tests, the roughness can have an influence up to large thicknesses. The rougher the surface, the more the roughness influences the results [69]. The proposed analysis does not consider the adherends surface treatment and roughness. As a matter of fact, it is assumed that the failure of the joint is always cohesive as often considered in the field of adhesive bonding.

Adhesive joints are subjected in some applications to dynamic loading, not addressed by the current selection procedure dealing only with static loading. When subjected to fatigue loading, fatigue life is also dependent upon the adherend properties, dimensions and joint geometry [70, 71]. This would require collecting a large amount of data which are not always available for the adhesives for which toughness data can be found in the literature.

On the mechanical description side, the first element of generalization that would improve the relevance of the analysis, but at the price of more complexity, is to account for mixed-mode cracking. Here, only mode I cracking from an internal pre-crack of length $2a$ is considered. The problem of Figure 2 should ideally account for the impact of the shear load on generating a K_{II} component that combines with K_I to set the crack driving force. Taking mixed-mode into account is possible if toughness values are known for different mode-mixities, which is rarely the case (at least for publicly available data), going back to a previous comment on the availability of rich mechanical databases for adhesives. The second element is regarding the architected joints, to develop models to predict the shear stiffness and thickness dependent strength for failure initiating at corners or collect experimental data, in order to provide a more realistic view on the potential of such solutions.

Many results show that the selection very much depends on crack length. A tacit assumption in our analysis, is that the crack size is material independent. This might not be true. The representative crack length could potentially be adhesive dependent due to the different type of chemistry and curing schedule. The problem of identification of the proper crack size is a remnant problem in all structural integrity assessment problems, especially with structural adhesive joints and very much connected to the capacity to estimate/measure the size of internal defects with non-destructive methods.

Regarding the considered crack configuration (centered crack through the thickness), one extension of the study would be to address other configurations or several crack positions in the joints: near the interface, in the bondline, at the center of the joint, at the edges. Indeed, several types of defects and damages can be found in adhesive joints. Some defects develop during the manufacturing phase such as voids due to entrapped air or kissing bonds which are located in the bondline and not especially close to the edges. Some damage also develops the in-service life due to mechanical loading or environment leading to crack developing along the edges. Depending on the crack position, the strength of the joint will vary as the expression of the geometric factor Y in Equation 3 is geometry dependent. This could possibly influence the ranking process by shifting the transition between the strength- and toughness-dominated regimes.

In order to set the bases of the selection approach, several arbitrary choices have been made regarding the models used to predict the tensile strength, the shear strength and the shear stiffness that affect the results. However, other models have also been developed in the literature and could be used. Alternatively, the selection tool could be coupled with finite element analyses. The choice of the different models has been based on the information available for the adhesives of the database but also on their predictive potential. In addition, some models are relevant for brittle adhesives but not for ductile ones and the opposite is also true. Introducing other models is thus left for further development of the selection procedure.

7. Conclusion

A method for selecting the best adhesive system has been worked out following Ashby's approach, accounting for the impact of the bond line thickness on the performance of the joint. The objectives that have been considered include: mass minimization, maximization of fracture toughness or maximization of the tensile load applied to the assembly. The constraints include: no failure under prescribed tensile and shear loading as well as an imposed minimum shear stiffness. Different loading configurations have been analyzed taking into account the presence of an internal crack and the presence of corners at the interface between adhesive and adherend. Both elementary and advanced models have been used to predict the effective strength of the joint including or not adherend effects as well as a fracture process zone effect. A database of adhesive properties with thickness dependence has been compiled to effectively apply the selection analysis. The key findings of the work are the following:

- The selection is very much dependent on crack length, leading to non-trivial choices with some adhesive performing better for short cracks and other for long cracks. This raises the remnant difficulty in structural integrity assessment based on fracture mechanics: How to precisely determine a relevant crack length? Progress in non-destructive analysis of adhesive joints [5] have been made to determine the defect sizes, but not all defects, such as weak bonds, can be detected [72].
- Working at the top fracture toughness requires the optimum adhesive thickness. But the optimum thickness is sometimes large, especially in very tough adhesives. A large thickness leads to a lower resistance to fracture from corners under tensile and shear loads. Also, thicker joints are less stiff in shear which is sometimes a

constraint in some applications. Subtle trade-offs have been found showing that the best adhesive choice varies from one problem to another.

- The use of advanced models taking the adherend stiffness into account is important [37, 73]. Indeed, a given adhesive tends to be selected for a larger crack length and a larger shear strength if E_s increases. In addition, taking the adherend stiffness into account can change the selection when having adhesives with almost equal K_{Ic} and σ_a^f. With the elementary model, the adhesive with the largest K_{Ic} is selected while, with a more advanced model, the one with the lowest E_a is selected.
- The selection method reveals gaps in the adhesive property charts: (i) a region with both stiff and tough adhesives and, (ii) a region with both strong and tough adhesives indicating the need for further possible improvements.
- The selection approach has been applied to architected joints with stop holes. Stop holes induce larger G_{Ic}, extending the range of adhesive performances. Such joints offer thus improved damage tolerance at lightweight, but at lower shear strength and stiffness.

Several directions have been proposed to enrich the present selection analysis to make it more versatile and more general.

Supplementary material

As supplementary material, a MATLAB application is available following the link: https://www.dropbox.com/scl/fo/guxcginsvkhyfqfkpnc1w/h?dl=0&rlkey=rl4190wb1p3bpu7stcuhsehlv .This allows the determination of the adhesive to select depending on the loading configuration. It runs based on the .csv and .txt files containing the information of Table 1. The current version only considers the elementary analysis in order to let it run for reasonable amount of time. Including the advanced models results in computations lasting for more than 1h instead of maximum 2 minutes.

Acknowledgments

CvI is a FRIA grantee of the Fonds de la Recherche Scientifique de Belgique - FNRS and gratefully acknowledges their support. The authors gratefully acknowledge Frederik Van Loock, Michal K. Budzik and Norman A. Fleck for interesting discussions and suggestions.

Declaration of competing interests

The authors declare that they have no known competing financial interests or personal relationships that could have appeared to influence the work reported in this paper.

Data availability

All the data used for this work can be found in the supplementary material.

References

[1] Pocius, A. V. *Adhesion and Adhesives Technology*, Third Edit.; KG, C. H. V. G. & C., Ed.; Carl Hanser Verlag GmbH & Co. KG, 2012. https://doi.org/10.3139/9783446431775.fm.

[2] Fisher, L. W. Selection of Engineering Materials and Adhesives. *Sel. Eng. Mater. Adhes.*, **2005**, 1–608. https://doi.org/10.1201/b15905.

[3] Weitzenböck, J. R. Selecting Adhesives for Marine Environments and Pre-Design. *Adhes. Mar. Eng.*, **2012**, 19–33. https://doi.org/10.1533/9780857096159.1.19.

[4] Suárez, J. C.; Diez de Ulzúrrun, I.; Biezma, M. V.; Ruiz Román, J. M.; Martínez, M. A.; Del Real, J. C.; López, F. Case Studies in Adhesives Selection. *J. Mater. Process. Technol.*, **2003**, *143–144* (1), 219–224. https://doi.org/10.1016/S0924-0136(03)00428-X.

[5] da Silva, L. F. M.; Öchsner, A.; Adams, R. D. *Handbook of Adhesion Technology: Second Edition*; 2018; Vol. 1–2. https://doi.org/10.1007/978-3-319-55411-2.

[6] Kinloch, A. J.; Shaw, S. J. The Fracture Resistance of a Toughened Epoxy Adhesive. *J. Adhes.*, **1981**, *12* (1), 59–77. https://doi.org/https://doi.org/10.1080/00218468108071189.

[7] Martiny, P.; Lani, F.; Kinloch, A. J.; Pardoen, T. A Multiscale Parametric Study of Mode i Fracture in Metal-to-Metal Low-Toughness Adhesive Joints. *Int. J. Fract.*, **2012**, *173* (2), 105–133. https://doi.org/10.1007/s10704-011-9667-x.

[8] Pardoen, T.; Ferracin, T.; Landis, C. M.; Delannay, F. Constraint Effects in

Adhesive Joint Fracture. *J. Mech. Phys. Solids*, **2005**, *53* (9), 1951–1983. https://doi.org/10.1016/j.jmps.2005.04.009.

[9] Wang, S. S.; Mandell, J. F.; McGarry, F. J. An Analysis of the Crack Tip Stress Field in DCB Adhesive Fracture Specimens. *Int. J. Fract.*, **1978**, *14* (1), 39–58. https://doi.org/10.1007/BF00032383.

[10] Chai, H. Bond Thickness Effect in Adhesive Joints and Its Significance for Mode I Interlaminar Fracture of Composites. *ASTM Spec. Tech. Publ.*, **1986**, No. July, 209–231. https://doi.org/10.1520/stp35350s.

[11] Bascom, W. D.; Cottington, R. L.; Jones, R. L.; Peyser, P. The Fracture of Epoxy- and Elastomer-modified Epoxy Polymers in Bulk and as Adhesives. *J. Appl. Polym. Sci.*, **1975**, *19* (9), 2545–2562. https://doi.org/10.1002/app.1975.070190917.

[12] Ranade, S. R.; Guan, Y.; Ohanehi, D. C.; Dillard, J. G.; Batra, R. C.; Dillard, D. A. A Tapered Bondline Thickness Double Cantilever Beam (DCB) Specimen Geometry for Combinatorial Fracture Studies of Adhesive Bonds. *Int. J. Adhes. Adhes.*, **2014**, *55*, 155–160. https://doi.org/10.1016/j.ijadhadh.2014.08.006.

[13] Daghyani, H. R.; Ye, L.; Mai, Y. W. Effect of Thermal Residual Stress on the Crack Path in Adhesively Bonded Joints. *J. Mater. Sci.*, **1996**, *31* (10), 2523–2529. https://doi.org/10.1007/BF00687277.

[14] Ji, G.; Ouyang, Z.; Li, G.; Ibekwe, S.; Pang, S. S. Effects of Adhesive Thickness on Global and Local Mode-I Interfacial Fracture of Bonded Joints. *Int. J. Solids Struct.*, **2010**, *47* (18–19), 2445–2458. https://doi.org/10.1016/j.ijsolstr.2010.05.006.

[15] Campilho, R. D. S. G.; Moura, D. C.; Banea, M. D.; da Silva, L. F. M. Adhesive Thickness Effects of a Ductile Adhesive by Optical Measurement Techniques. *Int. J. Adhes. Adhes.*, **2015**, *57* (March), 125–132. https://doi.org/10.1016/j.ijadhadh.2014.12.004.

[16] Martiny, P.; Lani, F.; Kinloch, A. J.; Pardoen, T. A Maximum Stress at a Distance Criterion for the Prediction of Crack Propagation in Adhesively-Bonded Joints. *Eng. Fract. Mech.*, **2013**, *97*, 105–135. https://doi.org/https://doi.org/10.1016/j.engfracmech.2012.10.025.

[17] Carbas, R. J. C.; Dantas, M. A.; Marques, E. A. S.; da Silva, L. F. M. Effect of the Adhesive Thickness on Butt Adhesive Joints under Torsional Loads. *J. Adv. Join. Process.*, **2021**, *3* (April), 100061. https://doi.org/10.1016/j.jajp.2021.100061.

[18] Davies, P.; Sohier, L.; Cognard, J. Y.; Bourmaud, A.; Choqueuse, D.; Rinnert, E.; Créac'hcadec, R. Influence of Adhesive Bond Line Thickness on Joint Strength. *Int. J. Adhes. Adhes.*, **2009**, *29* (7), 724–736. https://doi.org/10.1016/j.ijadhadh.2009.03.002.

[19] Naito, K.; Onta, M.; Kogo, Y. The Effect of Adhesive Thickness on Tensile and Shear Strength of Polyimide Adhesive. *Int. J. Adhes. Adhes.*, **2012**, *36*, 77–85. https://doi.org/10.1016/j.ijadhadh.2012.03.007.

[20] Arenas, J. M.; Narbón, J. J.; Alía, C. Optimum Adhesive Thickness in Structural Adhesives Joints Using Statistical Techniques Based on Weibull Distribution. *Int. J. Adhes. Adhes.*, **2010**, *30* (3), 160–165. https://doi.org/10.1016/j.ijadhadh.2009.12.003.

[21] da Silva, L. F. M.; Rodrigues, T. N. S. S.; Figueiredo, M. A. V.; de Moura, M. F. S. F.; Chousal, J. A. G. Effect of Adhesive Type and Thickness on the Lap Shear Strength. *J. Adhes.*, **2006**, *82* (11), 1091–1115. https://doi.org/10.1080/00218460600948511.

[22] Liu, Y.; Carnegie, C.; Ascroft, H.; Li, W.; Han, X.; Guo, H.; Hughes, D. J. Investigation of Adhesive Joining Strategies for the Application of a Multi-Material Light Rail Vehicle. *Materials (Basel).*, **2021**, *14* (22), 1–15. https://doi.org/10.3390/ma14226991.
[23] Reedy, E. D.; Guess, T. R. Butt Joint Tensile Strength: Interface Corner Stress Intensity Factor Prediction. *J. Adhes. Sci. Technol.*, **1995**, *9* (2), 237–251. https://doi.org/10.1163/156856195X01148.
[24] Ashby, M. F. *Materials Selection in Mechanical Design*, 5th ed.; Green, T., Ed.; Butterworth-Heinemann: Oxford, 2017. https://doi.org/10.1016/b978-1-85617-663-7.00026-6.
[25] Ashby, M. F.; Bréchet, Y. J. M. Designing Hybrid Materials. *Acta Mater.*, **2003**, *51* (19), 5801–5821. https://doi.org/10.1016/S1359-6454(03)00441-5.
[26] Heide-Jørgensen, S.; Teixeira de Freitas, S.; Budzik, M. K. On the Fracture Behaviour of CFRP Bonded Joints under Mode I Loading: Effect of Supporting Carrier and Interface Contamination. *Compos. Sci. Technol.*, **2018**, *160*, 97–110. https://doi.org/https://doi.org/10.1016/j.compscitech.2018.03.024.
[27] Maloney, K.; Fleck, N. Toughening Strategies in Adhesive Joints. *Int. J. Solids Struct.*, **2019**, *158*, 66–75. https://doi.org/10.1016/j.ijsolstr.2018.08.028.
[28] Heide-Jørgensen, S.; Budzik, M. K. Crack Growth along Heterogeneous Interface during the DCB Experiment. *Int. J. Solids Struct.*, **2017**, *120*, 278–291. https://doi.org/10.1016/j.ijsolstr.2017.05.013.
[29] Heide-Jørgensen, S.; Budzik, M. K.; Turner, K. T. Mechanics and Fracture of Structured Pillar Interfaces. *J. Mech. Phys. Solids*, **2020**, *137*, 103825. https://doi.org/10.1016/j.jmps.2019.103825.
[30] Athanasiadis, A. E. F.; Dias, M. A.; Budzik, M. K. Can Confined Mechanical Metamaterials Replace Adhesives? *Extrem. Mech. Lett.*, **2021**, *48*, 101411. https://doi.org/10.1016/j.eml.2021.101411.
[31] Tao, R.; Li, X.; Yudhanto, A.; Alfano, M.; Lubineau, G. On Controlling Interfacial Heterogeneity to Trigger Bridging in Secondary Bonded Composite Joints: An Efficient Strategy to Introduce Crack-Arrest Features. *Compos. Sci. Technol.*, **2020**, *188* (December 2019), 107964. https://doi.org/10.1016/j.compscitech.2019.107964.
[32] Morano, C.; Zavattieri, P.; Alfano, M. Tuning Energy Dissipation in Damage Tolerant Bio-Inspired Interfaces. *J. Mech. Phys. Solids*, **2020**, *141*, 103965. https://doi.org/10.1016/j.jmps.2020.103965.
[33] Banea, M. D.; Da Silva, L. F. M.; Campilho, R. D. S. G. The Effect of Adhesive Thickness on the Mechanical Behavior of a Structural Polyurethane Adhesive. *J. Adhes.*, **2014**, *91* (5), 331–346. https://doi.org/10.1080/00218464.2014.903802.
[34] Reis, P. N. B.; Ferreira, J. A. M.; Antunes, F. Effect of Adherends Rigidity on the Shear Strength of Single Lap Adhesive Joints. *Int. J. Adhes. Adhes.*, **2011**, *31* (4), 193–201. https://doi.org/10.1016/j.ijadhadh.2010.12.003.
[35] da Silva, L. F. M.; Carbas, R. J. C.; Critchlow, G. W.; Figueiredo, M. A. V.; Brown, K. Effect of Material, Geometry, Surface Treatment and Environment on the Shear Strength of Single Lap Joints. *Int. J. Adhes. Adhes.*, **2009**, *29* (6), 621–632. https://doi.org/10.1016/j.ijadhadh.2009.02.012.
[36] Van Loock, F.; Thouless, M. D.; Fleck, N. A. Tensile Fracture of an Adhesive Joint: The Role of Crack Length and of Material Mismatch. *J. Mech. Phys. Solids*, **2019**, *130*, 330–348. https://doi.org/10.1016/j.jmps.2019.06.004.
[37] Askarinejad, S.; Thouless, M. D.; Fleck, N. A. Failure of a Pre-Cracked Epoxy Sandwich Layer in Shear. *Eur. J. Mech. A/Solids*, **2021**, *85* (October 2020),

104134. https://doi.org/10.1016/j.euromechsol.2020.104134.

[38] Akisanya, A. R.; Fleck, N. A. Interfacial Cracking from the Free-Edge of a Long Bi-Material Strip. *Int. J. Solids Struct.*, **1997**, *34* (13), 1645–1665. https://doi.org/10.1016/S0020-7683(96)00053-4.

[39] Chen, K.; Wu, Y.; Han, W.; Liu, B.; Wenjie, W.; Liu, H.; Li, Y. Influence of Adhesive Thickness and Defect on Mechanical Property of Adhesive Bonded Joint of Flexible Polymer Substrate and Cable for Solar Panel Application. *Int. J. Adhes. Adhes.*, **2023**, *126* (March), 103485. https://doi.org/10.1016/j.ijadhadh.2023.103485.

[40] Guo, L.; Liu, J.; Xia, H.; Li, X.; Zhang, X.; Yang, H.; Yang, Y. Effects of Loading Rate, Temperature, and Thickness on the Tensile Strength of Precision Adhesive Joints. *Polym. Test.*, **2022**, *109* (January), 107528. https://doi.org/10.1016/j.polymertesting.2022.107528.

[41] Campilho, R. D. S. G.; Moura, D. C.; Banea, M. D.; da Silva, L. F. M. Adherend Thickness Effect on the Tensile Fracture Toughness of a Structural Adhesive Using an Optical Data Acquisition Method. *Int. J. Adhes. Adhes.*, **2014**, *53*, 15–22. https://doi.org/10.1016/j.ijadhadh.2014.01.015.

[42] da Silva, L. F. M.; das Neves, P. J. C.; Adams, R. D.; Wang, A.; Spelt, J. K. Analytical Models of Adhesively Bonded Joints-Part II: Comparative Study. *Int. J. Adhes. Adhes.*, **2009**, *29* (3), 331–341. https://doi.org/10.1016/j.ijadhadh.2008.06.007.

[43] Stein, N.; Weißgraeber, P.; Becker, W. A Model for Brittle Failure in Adhesive Lap Joints of Arbitrary Joint Configuration. *Compos. Struct.*, **2015**, *133*, 707–718. https://doi.org/10.1016/j.compstruct.2015.07.100.

[44] Groth, H. L. Stress Singularities and Fracture at Interface Corners in Bonded Joints. *Int. J. Adhes. Adhes.*, **1988**, *8* (2), 107–113. https://doi.org/10.1016/0143-7496(88)90031-0.

[45] Van Tooren, M. J. L.; Gleich, D. M.; Beukers, A. Experimental Verification of a Stress Singularity Model to Predict the Effect of Bondline Thickness on Joint Strength. *J. Adhes. Sci. Technol.*, **2004**, *18* (4), 395–412. https://doi.org/10.1163/156856104323016315.

[46] Goglio, L.; Rossetto, M. Stress Intensity Factor in Bonded Joints: Influence of the Geometry. *Int. J. Adhes. Adhes.*, **2010**, *30* (5), 313–321. https://doi.org/10.1016/j.ijadhadh.2009.12.008.

[47] Akhavan-Safar, A.; Ayatollahi, M. R.; Rastegar, S.; da Silva, L. F. M. Impact of Geometry on the Critical Values of the Stress Intensity Factor of Adhesively Bonded Joints. *J. Adhes. Sci. Technol.*, **2017**, *31* (18), 2071–2087. https://doi.org/10.1080/01694243.2017.1297064.

[48] Boutar, Y.; Naïmi, S.; Mezlini, S.; Da Silva, L. F. M.; Hamdaoui, M.; Ben Sik Ali, M. Effect of Adhesive Thickness and Surface Roughness on the Shear Strength of Aluminium One-Component Polyurethane Adhesive Single-Lap Joints for Automotive Applications. *J. Adhes. Sci. Technol.*, **2016**, *30* (17), 1913–1929. https://doi.org/10.1080/01694243.2016.1170588.

[49] Pardoen, T.; Turner, K. T.; Budzik, M. K. Architected Adhesive Joints with Improved Fracture Toughness. In *Advances in Structural Adhesive Bonding*; Dillard, D. A., Ed.; Woodhead Publishing Series in Materials, 2023; pp 1105–1122.

[50] Dupont. *DuPont Provides Lightweight Bonding Solutions for Aston Martin ' s First-Ever Luxury SUV*; 2020.

[51] Budzik, M. K.; Wolfahrt, M.; Reis, P.; Kozłowski, M.; Sena-Cruz, J.; Papadakis,

L.; Nasr Saleh, M.; Machalicka, K. V.; Teixeira de Freitas, S.; Vassilopoulos, A. P. Testing Mechanical Performance of Adhesively Bonded Composite Joints in Engineering Applications: An Overview. *J. Adhes.*, **2022**, *98* (14), 2133–2209. https://doi.org/10.1080/00218464.2021.1953479.

[52] Heide-Jørgensen, S.; Budzik, M. K. Effects of Bondline Discontinuity during Growth of Interface Cracks Including Stability and Kinetic Considerations. *J. Mech. Phys. Solids*, **2018**, *117*, 1–21. https://doi.org/10.1016/j.jmps.2018.04.002.

[53] Sun, C.; Thouless, M. D.; Waas, A. M.; Schroeder, J. A.; Zavattieri, P. D. Ductile-Brittle Transitions in the Fracture of Plastically Deforming, Adhesively Bonded Structures. Part II: Numerical Studies. *Int. J. Solids Struct.*, **2008**, *45* (17), 4725–4738. https://doi.org/10.1016/j.ijsolstr.2008.04.007.

[54] Pascuzzo, A.; Yudhanto, A.; Alfano, M.; Lubineau, G. On the Effect of Interfacial Patterns on Energy Dissipation in Plastically Deforming Adhesive Bonded Ductile Sheets. *Int. J. Solids Struct.*, **2020**, *198*, 31–40. https://doi.org/10.1016/j.ijsolstr.2020.04.001.

[55] Maloney, K.; Fleck, N. Damage Tolerance of an Architected Adhesive Joint. *Int. J. Solids Struct.*, **2018**, *132–133*, 9–19. https://doi.org/10.1016/j.ijsolstr.2017.06.010.

[56] Zavattieri, P. D.; Hector, L. G.; Bower, A. F. Determination of the Effective Mode-I Toughness of a Sinusoidal Interface between Two Elastic Solids. *Int. J. Fract.*, **2007**, *145* (3), 167–180. https://doi.org/10.1007/s10704-007-9109-y.

[57] Cordisco, F. A.; Zavattieri, P. D.; Hector, L. G.; Carlson, B. E. Mode I Fracture along Adhesively Bonded Sinusoidal Interfaces. *Int. J. Solids Struct.*, **2016**, *83*, 45–64. https://doi.org/10.1016/j.ijsolstr.2015.12.028.

[58] Yudhanto, A.; Almulhim, M.; Kamal, F.; Tao, R.; Fatta, L.; Alfano, M.; Lubineau, G. Enhancement of Fracture Toughness in Secondary Bonded CFRP Using Hybrid Thermoplastic/Thermoset Bondline Architecture. *Compos. Sci. Technol.*, **2020**, *199* (July), 108346. https://doi.org/10.1016/j.compscitech.2020.108346.

[59] Owens, J. F. P.; Lee-sullivan, P. Stiffness Behaviour Due to Fracture in Adhesively Bonded Composite-to-Aluminum Joints II. Experimental. **2000**, *20*.

[60] Owens, J. F. P.; Lee-Sullivan, P. Stiffness Behaviour Due to Fracture in Adhesively Bonded Composite-to-Aluminum Joints: I. Theoretical Model. *Int. J. Adhes. Adhes.*, **2000**, *20* (1), 39–45. https://doi.org/10.1016/S0143-7496(99)00013-5.

[61] Quispe Rodríguez, R.; De Paiva, W. P.; Sollero, P.; Bertoni Rodrigues, M. R.; De Albuquerque, É. L. Failure Criteria for Adhesively Bonded Joints. *Int. J. Adhes. Adhes.*, **2012**, *37* (September), 26–36. https://doi.org/10.1016/j.ijadhadh.2012.01.009.

[62] Tserpes, K.; Barroso-Caro, A.; Carraro, P. A.; Beber, V. C.; Floros, I.; Gamon, W.; Kozłowski, M.; Santandrea, F.; Shahverdi, M.; Skejić, D.; et al. A Review on Failure Theories and Simulation Models for Adhesive Joints. *J. Adhes.*, **2022**, *98* (12), 1855–1915. https://doi.org/10.1080/00218464.2021.1941903.

[63] da Silva, L. F. M.; Campilho, R. D. S. G. *Advances in Numerical Modelling of Adhesive Joints*; 2012. https://doi.org/10.1007/978-3-642-23608-2_1.

[64] Granta. Granta EduPack 2021 R2. Cambridge 2021.

[65] Tao, R.; Li, X.; Yudhanto, A.; Alfano, M.; Lubineau, G. Toughening Adhesive Joints through Crack Path Engineering Using Integrated Polyamide Wires. *Compos. Part A Appl. Sci. Manuf.*, **2022**, *158* (April), 106954. https://doi.org/10.1016/j.compositesa.2022.106954.

[66] Shahid, M.; Hashim, S. A. Effect of Surface Roughness on the Strength of Cleavage Joints. *Int. J. Adhes. Adhes.*, **2002**, *22* (3), 235–244. https://doi.org/10.1016/S0143-7496(01)00059-8.
[67] Paz, E.; Narbón, J. J.; Abenojar, J.; Cledera, M.; del Real, J. C. Influence of Acrylic Adhesive Viscosity and Surface Roughness on the Properties of Adhesive Joint. *J. Adhes.*, **2016**, *92* (11), 877–891. https://doi.org/10.1080/00218464.2015.1051221.
[68] Molitor, P.; Barron, V.; Young, T. *Surface Treatment of Titanium for Adhesive Bonding to Polymer Composites: A Review*; 2001; Vol. 21.
[69] Zarei, H.; Rosaria Marulli, M.; Paggi, M.; Pietrogrande, R.; Üffing, C.; Weißgraeber, P. Adherend Surface Roughness Effect on the Mechanical Response of Silicone-Based Adhesive Joints. *Eng. Fract. Mech.*, **2020**, *240* (May). https://doi.org/10.1016/j.engfracmech.2020.107353.
[70] Azari, S.; Papini, M.; Spelt, J. K. Effect of Adhesive Thickness on Fatigue and Fracture of Toughened Epoxy Joints - Part II: Analysis and Finite Element Modeling. *Eng. Fract. Mech.*, **2011**, *78* (1), 138–152. https://doi.org/10.1016/j.engfracmech.2010.07.006.
[71] Sahin, R.; Akpinar, S. The Effects of Adherend Thickness on the Fatigue Strength of Adhesively Bonded Single-Lap Joints. *Int. J. Adhes. Adhes.*, **2021**, *107* (March), 102845. https://doi.org/10.1016/j.ijadhadh.2021.102845.
[72] Omairey, S.; Jayasree, N.; Kazilas, M. Defects and Uncertainties of Adhesively Bonded Composite Joints. *SN Appl. Sci.*, **2021**, *3* (9). https://doi.org/10.1007/s42452-021-04753-8.
[73] Loock, F. Van. Deformation and Fracture of PMMA with Application to Nanofoaming and Adhesive Joints. **2019**, No. April.
[74] ISO. *ISO25217 Adhesives — Determination of the Mode 1 Adhesive Fracture Energy of Structural Adhesive Joints Using Double Cantilever Beam and Tapered Double Cantilever Beam Specimens*; 2014.
[75] Carlberger, T.; Stigh, U. Influence of Layer Thickness on Cohesive Properties of an Epoxy-Based Adhesive-an Experimental Study. *J. Adhes.*, **2010**, *86* (8), 816–835. https://doi.org/10.1080/00218464.2010.498718.
[76] Chai, H. Bond Thickness Effect in Mixed-Mode Fracture and Its Significance to Delamination Resistance. *Int. J. Solids Struct.*, **2021**, *219–220*, 63–80. https://doi.org/10.1016/j.ijsolstr.2021.03.006.
[77] Lee, D. B.; Ikeda, T.; Miyazaki, N.; Choi, N. S. Effect of Bond Thickness on the Fracture Toughness of Adhesive Joints. *J. Eng. Mater. Technol.*, **2004**, *126* (1), 14–18. https://doi.org/10.1115/1.1631433.
[78] Marzi, S.; Biel, A.; Stigh, U. On Experimental Methods to Investigate the Effect of Layer Thickness on the Fracture Behavior of Adhesively Bonded Joints. *Int. J. Adhes. Adhes.*, **2011**, *31* (8), 840–850. https://doi.org/10.1016/j.ijadhadh.2011.08.004.
[79] Hutchinson, J. W.; Tvergaard, V. The Relation between Crack Growth Resistance and Fracture Process Parameters Elastic-Plastic Solids. *J. Mech. Phys. Solids*, **1992**, *40* (6), 1377–1397.
[80] Chai, H. Fracture Work of Thin Bondline Adhesive Joints. *J. Mater. Sci. Lett.*, **1988**, *7* (4), 399–401. https://doi.org/10.1007/BF01730756.
[81] Chai, H. Deformation and Fracture of Particulate Epoxy in Adhesive Bonds. *Acta Metall. Mater.*, **1995**, *43* (1), 163–172. https://doi.org/10.1016/0956-7151(94)00216-5.
[82] Ben Salem, N.; Budzik, M. K.; Jumel, J.; Shanahan, M. E. R.; Lavelle, F.

Investigation of the Crack Front Process Zone in the Double Cantilever Beam Test with Backface Strain Monitoring Technique. *Eng. Fract. Mech.*, **2013**, *98* (1), 272–283. https://doi.org/10.1016/j.engfracmech.2012.09.028.

Appendix A: Derivation of $A_p(\nu)$ and λ in butt tensile joints

Reedy and Guess [23] derived a model based on an interface corner stress intensity factor to predict σ^{f*}, assuming that failure only takes place near the interface and that the joint is free from any defect. In tensile butt joints, the interface corner stress singularity order is $\lambda - 1$. The joint tensile strength is given by Eq. 10 which depends on $A_p(\nu)$ and λ. Values of $A_p(\nu)$ have been tabulated by Reedy and Guess and can be found in [23]. Regarding the order of the singularity, it depends upon the Dundur's parameters α and β. λ can be determined by solving the Eq. A1 derived by Akisanya and Fleck [38]:

$$\begin{gathered}16(\mu-1)^2\left[\lambda^2-\sin^2\left(\frac{\lambda\pi}{2}\right)^2\right]-4[\mu(\kappa_s+1)-(\kappa_a+1)]^2\left[\lambda^2-\sin^4\left(\frac{\lambda\pi}{2}\right)\right]\\+16(\mu-1)\sin^2\left(\frac{\lambda\pi}{2}\right)[\mu(\kappa_s+1)-(\kappa_a+1)]\left[\lambda^2-\sin^2\left(\frac{\lambda\pi}{2}\right)\right]\\+[\mu(\kappa_s+1)+(\kappa_a+1)]^2\sin^2(\lambda\pi)=0\end{gathered} \qquad (A1)$$

where $\mu = \mu_a/\mu_s$ with $\mu_i = E_i/2(1+\nu_i)$ the shear modulus of material *i* and the shear coefficient *i* $\kappa_i = 3 - 4\nu_i$.

Appendix B: Derivation of λ for TAST configuration

Askarinejad et al. [37] developed a fracture mechanics methodology for the failure of elastic-brittle lap-shear joints based on the TAST configuration. This model depends on two parameters: b and λ. The value of b depends on the joint geometry and on the adhesive and adherends shear modulus and Poisson ratio while α and β are the Dundurs parameters. The authors determined b by calibrating the model on experimental data.

Hence, b can be obtained based on the shear strength of the joint for at least two different thicknesses. However, these data are not available for the adhesives entering our database (section 3.4). The singularity order is also dependent upon adherends Young's modulus and Poisson ratio and can be determined by finding the root of

$$\begin{gathered} F(\lambda) = [(4(\kappa_a^2 - 4\lambda^2 + 1) + 8\kappa_a \cos(\pi\lambda)) \sin^2(\pi\lambda) \\ -2\mu^2\left((\cos(\pi\lambda) + 2\lambda^2 - 1)(4\kappa_s cos^2(\pi\lambda) + (\kappa_s - 1)^2)\right) \\ -4\mu\left((\kappa_S - 1)\left(4\lambda^2 sin^2(\pi\lambda) - (\kappa_s - 1)cos^2(\pi\lambda)\right)\right. \\ +(\kappa_a\kappa_s + 1)(1 - \sin(2\pi\lambda)\sin(\pi\lambda)) - \kappa_a - \kappa_s)]/4\sin^2(\pi\lambda) \end{gathered}, \qquad (B1)$$

where $\mu = \mu_a/\mu_s$ with $\mu_i = E_i/2(1+\nu_i)$ the shear modulus of material i and the shear coefficient i $\kappa_i = 3 - 4\nu_i$. For given geometric parameters and adherend and adhesives properties, the shear strength decreases thus as $t^{\lambda-1}$ and this decrease depends on the properties of both adherends and adhesive. The use of this relationship requires computing λ and b for several geometries and adherend-adhesive properties which is time consuming. For typical metal-adhesive systems, λ will tend to 0.63-0.65. The dependence of b is neglected in the current work.

Appendix C: Maximization of K_{Ic}

a) Classical adhesive joints

This scenario involves the maximization of the joint fracture toughness, with two constraints being put on the applied shear stress and the required shear stiffness. The two constraints are put as limits. Hence, the selected adhesive is the one that meets the shear strength and stiffness requirements and that maximizes K_{Ic} for t comprised between t_{min} and t_{max}. t_{min} is set to 200 µm while no limit is put on t_{max}. Figure C.1 shows the influence of τ^∞ and τ^∞/u_τ^{max} on the selection. First, it is important to note that the selection is independent of the crack length. Figure C.1 shows that increasing the applied shear stress leads to the selection of a stronger adhesive, but which is characterized by a lower maximum critical stress intensity factor (lighter color). If the required shear stiffness is now increased, stiffer adhesives tend to be selected. In addition, when the stiffness is increased, the maximum K_{Ic} that can be reached decreases. These two effects arise from the fact that stiff and strong adhesives tend to be brittle while soft and flexible ones are tougher (see Figure 6). For a given stiffness and for a given adhesive, the maximum K_{Ic} that can be reached is independent upon τ^{∞} as in the elementary level of analysis when minimizing the mass. However, for a given adhesive and a given required shear strength, increasing the stiffness leads to a reduction of the maximum K_{Ic} that can be reached. Indeed, as the stiffness increases, the maximum thickness for which the adhesive can be selected is decreased. If this thickness is lower than the thickness maximizing K_{Ic}, t^*, decreasing the stiffness leads to a decrease of the maximum K_{Ic}.

The parameters t_{min} and t_{max} also influence the selection as the adhesive fracture toughness evolves with the adhesive thickness. Increasing t_{min} results in a decrease of the maximum stiffness that can be reached in general and for each adhesive (Figure C.1a-b). Hence, stiffer adhesives tend to be selected for lower required stiffnesses. For given conditions, as long as t_{min} is below $t^*$and that the adhesive is of type A (Figure 2), the maximum K_{Ic} that can be reached is not affected. If now, there is a limit on t_{max}, the selection can be affected. Indeed, in Figure C.1c, SikaPower 498 cannot longer be selected because in the range going from t_{min} to t_{max}, the Betamate 1493 adhesive is the toughest. Due to the dependence of G_{Ic} on the adhesive thickness, t_{min} and t_{max} influence the selection of the adhesive maximizing K_{Ic}.

b) Architected joints with stop holes

The objective is now to maximize K_{Ic} for architected joints with stop holes. This objective is the one that motivated the design of such joints by Maloney and Fleck [27] and Heide-Jørgensen and Budzik [52]. The selection map is shown in Figure C.2. depending on the constraints on the shear stress and the shear stiffness. For low imposed shear stress and stiffnesses, the three architected joints containing 50%, 33% and 25% of cavities can be selected. Indeed, they all lead to the same fracture toughness. As the stiffness is increased, joints containing a large number of stop holes tend to no longer be selected. Indeed, the larger the number of cavities, the lower the true surface area over which the shear force acts, resulting in a lower stiffness. Consequently, for a given thickness, the joint containing 50% of cavities is less stiff than the one containing 33% and the maximum thickness for which it can be selected tends to be lower than t^* for a lower stiffness constraint. This results in a lower fracture toughness while the joints containing 33% and 25% can still have a thickness t^*, maximizing K_{Ic}. At some point, only the adhesive containing 25% of stop holes can be selected. However, when further increasing the stiffness, even if the selection thickness is lower than t^*, it remains tougher than the plain adhesive joint. At this point, it is observed that the maximum achieved K_{Ic} decreases. At some point, the required stiffness is high enough such that the thickness for which the 25% joint can be selected leads to a joint less tough than the plain adhesive joint. Regarding, the influence of the shear stress, when it is increased, joints containing large amount of cavities can no longer be selected and for large shear stress, only the plain adhesive joint can be selected resulting in more brittle joint. To conclude, architected joints with stop holes are an alternative to plain adhesive joints for limited strength and stiffness constraints.

Appendix D: Maximization of the remote tensile stress σ^{∞}

a) Classical adhesive joints

The remote tensile stress is now maximized for classical adhesive joints. As in the previous case, the two constraints are the shear stress and stiffness which are set as limits. The parameters entering the selection are thus *2a*, τ^{∞}, u_{τ}^{max}, t_{min} and t_{max}. Figure D.1. shows the influence of the crack length and the required shear stress on the selection for different required shear stiffnesses. The maximum tensile stress that can be reached depending on τ^{∞}, $\tau^{\infty}/u_{\tau}^{max}$ and *2a* is shown based on the color scale, the lighter the color, the lower the maximum σ^{∞} that can be applied. For short cracks and high shear strength, the strongest and stiffest adhesives are selected. For low shear strengths, if the crack length is longer, tougher adhesives start to be selected leading to the selection of the SikaPower 498 adhesive. However, these tough adhesives are often softer than the brittle one. Hence, when a high shear stress is applied, stronger adhesives such as the BP907 and the Araldite GY260 adhesives are selected. However, this is accompanied by a decrease in the maximum remote tensile load that can be applied on the joint as shown in Figure D.1d. The influence of the shear stiffness is considered by comparing Figure D.1a to c. By increasing the stiffness from 100 MPa/mm to 1000 MPa/mm, the SikaPower 498 adhesive cannot be selected due to its low shear modulus. Hence the Betamate 1493 adhesive is selected. Further increasing the required stiffness leads to the selection of only the ESP110 adhesive. The Betamate 73455 also meets the stiffness requirements but it is less strong and tough and is thus never the optimal adhesive to select. As the other adhesives do not meet the stiffness requirement, no adhesive can be selected for a required shear strength larger than 40 MPa.

As for the other scenarios, t_{min} and t_{max} can influence the selection as shown in Figure D.2. First t_{min} influence the maximum stiffness that can be reached. It t_{min} is increased, for a given required stiffness, the softest adhesive in Figure D.1b, Betamate 1493, is no longer selected and the F185 adhesive is then selected, as shown in Figure D.1a. In addition, when comparing Figure D.1b and B.2a, BP907 is selected for a lower range of thicknesses if t_{min} is increased. Figure D.2b shows the influence of t_{max} when compared to Figure D.1a. The SikaPower 498 adhesive is no longer selected being replaced by the Betamate 1493 adhesive. Due to the dependence of G_{Ic} on *t*, the selection is changed when varying t_{min} and t_{max}.

The objectives of maximizing σ^{∞} or K_{Ic} can now be compared. When K_{Ic} is maximized, the selection is independent on crack length. In both cases, increasing the imposed shear stress and the shear stiffness results in the selection of less tough adhesives. This arises from the fact that adhesives are either characterized by high strength and stiffness, but low toughness or high toughness and low strength and stiffness.

b) Architected adhesive joints with stop holes

As for classical adhesive joints, the goal is to maximize the applied tensile stress as a function of the applied shear and stiffness constraints and of the crack length. The selection map for shear stiffnesses lower than 4000 MPa/mm is shown in Figure D.3. For small cracks, the plain joint is selected. Indeed, at small crack length, the adhesive is first insensitive to defect size and the effective surface over which the tensile force acts is lower with cavities. Hence, the effective tensile strength is larger for a plain adhesive joint. When increasing crack length, the joint with 25% of stop holes is selected as the reduction of effective cross-section area is balanced by the improved fracture toughness coming from the crack blunting by the stop holes. However, joints with more stop holes tend not to be selected because they are characterized by a similar fracture toughness and lower effective cross-section resulting in a lower σ^{f*}. Due to this reduction in effective cross-section, the shear strength of the joint also decreases when inserting stop holes leading to the selection of the plain joint for applications involving large applied shear stresses. If the required shear stiffness exceeds 4000 MPa/mm, only the plain adhesive joint is selected.

Appendix E: Finite element model for architected joints with stop holes

In order to apply the selection approach to architected joints, simulations are run based on the design rules of Heide-Jørgensen and Budzik [52], using the finite element software Abaqus. The influence of the spacing between the stop holes, S_{archi}, and of the thickness is investigated. The length of the stop holes *D* is thus set to $2l_p$ (Eq. 23) while the spacing S_{archi} between them is set to $2l_p$, $4l_p$ and $6l_p$ to vary the number of cavities in the joint while *t* is varied from 0.1 to 1 mm. The influence of *D* and *t* on the joint fracture toughness is investigated by modelling a DCB specimen while a lap shear joint is modelled to consider their influence on the shear properties (Figure E.1). The implemented constitutive laws and failure criterion correspond to those of Martiny et al. [16]. The 4 mm thick adherends are thus modelled as mild steel and the adhesive as Betamate 73455. The crack propagates when the maximum principal stress ahead of the crack tip reaches 98 MPa over a distance of 18 µm. For both models, the mesh is generated using a Python script and the Gmsh API and is made of four nodes plane strain elements (CPE4R).

The DCB is 150 mm long with a pre-crack length of 50 mm (Figure E.1). The crack tip corresponds to the end of the first stop hole while two additional stop holes are inserted ahead of the crack tip. The edges of the stop holes are slightly rounded with a filet radius equal to the adhesive thickness to avoid large stress concentrations at the corners near the interface. The mesh is refined near the crack tip over a distance equal to t_a with elements of length between 1 and 5 µm. The simulations are run under controlled displacement with a displacement imposed on the left upper corner as shown in Figure E.1a. When the failure criterion is met, G_{Ic} is computed based on Eq. E.1 from the ISO 25217 standard [74], using the single beam theory and is given in Figure E.2b.

$$G_{Ic} = \frac{4P^2}{E_s W^2}\left(\frac{3a^2}{h_s^3} + \frac{1}{h_s}\right) . \qquad (E.1)$$

Symmetric lap shear joints (Figure E.1b) are modelled with 100 mm long arms overlapping over a distance of 12.7 mm. The number of cavities is adapted depending on the stop hole length and spacing. A horizontal displacement is prescribed at the left side of the joint while the right edge is clamped. The shear stiffness and is given in Figure E.2a.

List of abbreviations and symbols

a	Half crack length [mm]	m_a	Adhesive mass [kg]
a_c	Half critical crack length [mm]	m_{TC}	Objective function: mass and tensile constraint [kg]
a_{edge}	Length of edge crack [mm]	m_{SC1}	Objective function: mass and shear stiffness constraint [kg]
α	First Dundur's parameter	m_{SC2}	Objective function: mass and shear strength constraint [kg]
β	Second Dundur's parameter	μ_a	Adhesive shear modulus [MPa]
C	Cost [€]	μ_s	Adherend shear modulus
C_a	Mass cost of the adhesive [€/kg]	ρ_a	Adhesive density [kg/m³]
C_m	Joint manufacturing cost [€/m³]	ρ_s	Adherend density [kg/m³]
D	Stop hole length [mm]	S	Surface area of the joint [m²]
E_a	Adhesive Young's modulus [GPa]	S_{archi}	Spacing between stop holes [mm]
E_s	Adherends Young's modulus [GPa]	S_{holes}	Surface area occupied by stop holes when orthogonally projected [m²]
F_σ	Tensile force [N]	σ_a^f	Adhesive tensile strength [MPa]
F_τ	Shear force [N]	σ^{f*}	Effective tensile strength [MPa]
G_{Ic}	Adhesive fracture toughness [J/m²]	σ^∞	Remote tensile stress [MPa]
h_s	Adherends thickness [mm]	σ_{archi}^f	Tensile strength of architected joint [MPa]
K_{Ic}	Critical stress intensity factor $[MPa\sqrt{m}]$	σ_{0a}	Yield strength of the adhesive [MPa]
K_f	Interface corner stress intensity factor $[MPa\sqrt{m}]$	τ_a^f	Adhesive shear strength [MPa]
κ_i	Shear coefficient of material i (a or s)	τ^∞	Remote shear stress [MPa]
L_a	Adhesive length [m]	τ^{f*}	Effective shear strength [MPa]

L_{s1}	Top adherend length [m]	τ_{archi}^{f}	Shear strength of architected joint [MPa]
L_{s2}	Bottom adherend length [m]	u_{τ}	Shear displacement [mm]
l_s	Process zone length [mm]	u_{τ}^{max}	Maximum shear displacement [mm]
l_p	Process zone length for architected joints [mm]	ν_a	Adhesive Poisson ratio [-]
λ	Singularity order [-]	W	Joint width [m]
λ_w	Elastic foundation wave number [1/mm]	Y	Geometric factor
m	Joint mass [kg]		

Table 1: Equations used for the different loading configurations and levels of analysis

Loading	Elementary level	Advanced level
Tension	Eq. 1 and 3	- Eq. 4 is satisfied: is Eq. 6 satisfied? ○ Yes: $\sigma^{f*} = \sigma_a^f$ ○ No: Eq. 7 - Eq. 4 is not satisfied: ○ Eq. 8
Shear	Eq. 11	Eq. 12

Table 2: Adhesives entering the selection app for which literature data regarding the evolution of G_{Ic} can be found.

Adhesive	**Maximum fracture toughness (adhesive thickness) [J/m²] (mm)**	**Fracture toughness – plateau value [J/m²]**	**Young's modulus [GPa]**	**Tensile strength [MPa]**	**Source**
Araldite GY260	810 (0.5)	810	3.1	82	Daghyani et al. [13]
Betamate 1493	6240 (0.4)	6240	1.8	40	Martiny et al. [7]
Betamate 73455	220 (0.5)	210	6	25	Martiny et al. [7]
Betamate XW1044-3	1690 (1)	1500	2.9	35	Carlberger et al. [75]
BP907	800 (0.25)	520	3.2	90*	Chai [76]
ESP110	1480 (0.88)	1480	5.7	70	Martiny et al. [7]
F185	3445 (0.25)	3445	2.9	50	Chai [76]
FM1000	5280 (0.05)	4860	1.2	50*	Chai [76]
Loctite Hysol 9460	760 (1)	760	2.8	30	Ji et al. [14]
Lord 320/322	1020 (4.5)	1020	2.5	28	Ranade et al. [12]
Rubber modified epoxy	3100 (0.42)	2350	2.6	70*	Kinloch and Shaw[6]
Rubber modified epoxy	240 (2)	240	2.6	50*	Lee et al. [77]
Sikaforce 7752 L60	5240 (2)	5240	0.5	12	Campilho et al. [15]
SikaPower 498	6960 (2)	6960	2	30	Marzi et al. [78]

*Data not available: assumed from typical values found in the literature or estimated based on the knowledge of the glass transition temperature.

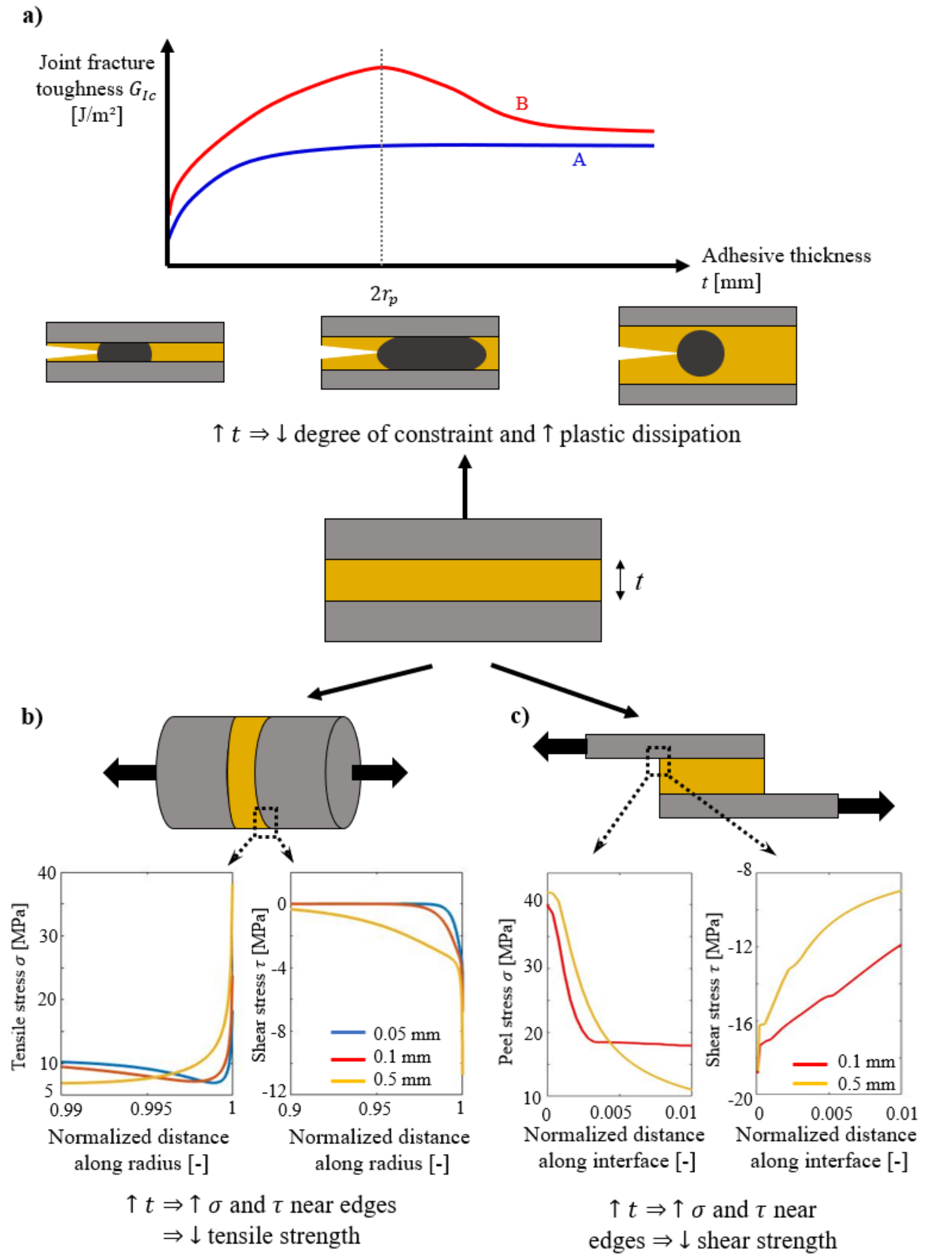
a)
Joint fracture toughness G_{Ic} [J/m²]
B
A
Adhesive thickness t [mm]
$2r_p$
↑ t ⇒ ↓ degree of constraint and ↑ plastic dissipation
t
b)
c)
Tensile stress σ [MPa]
Normalized distance along radius [-]
Shear stress τ [MPa]
0.05 mm
0.1 mm
0.5 mm
Normalized distance along radius [-]
Peel stress σ [MPa]
Normalized distance along interface [-]
Shear stress τ [MPa]
0.1 mm
0.5 mm
Normalized distance along interface [-]
↑ t ⇒ ↑ σ and τ near edges ⇒ ↓ tensile strength
↑ t ⇒ ↑ σ and τ near edges ⇒ ↓ shear strength

Figure 1

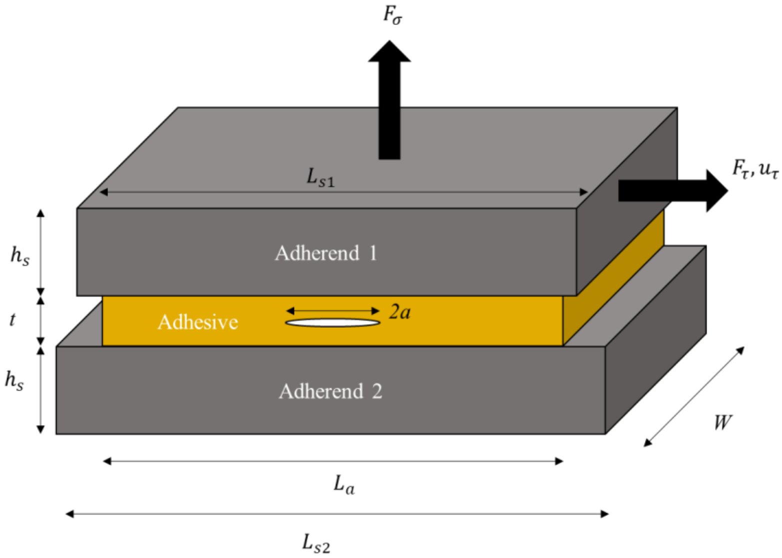

Figure 2

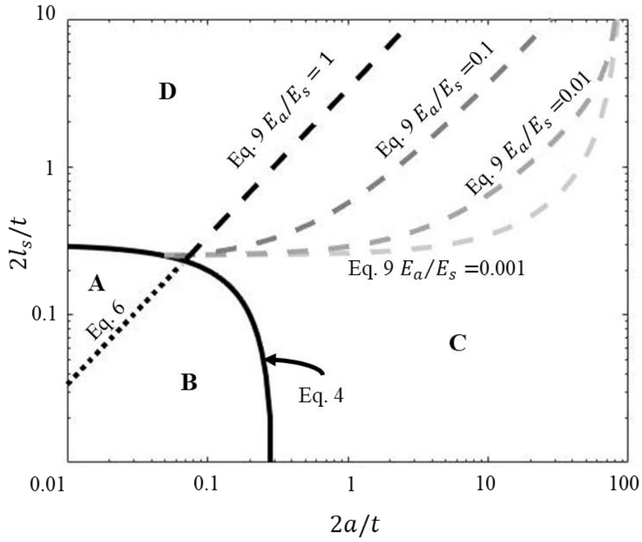

Figure 3

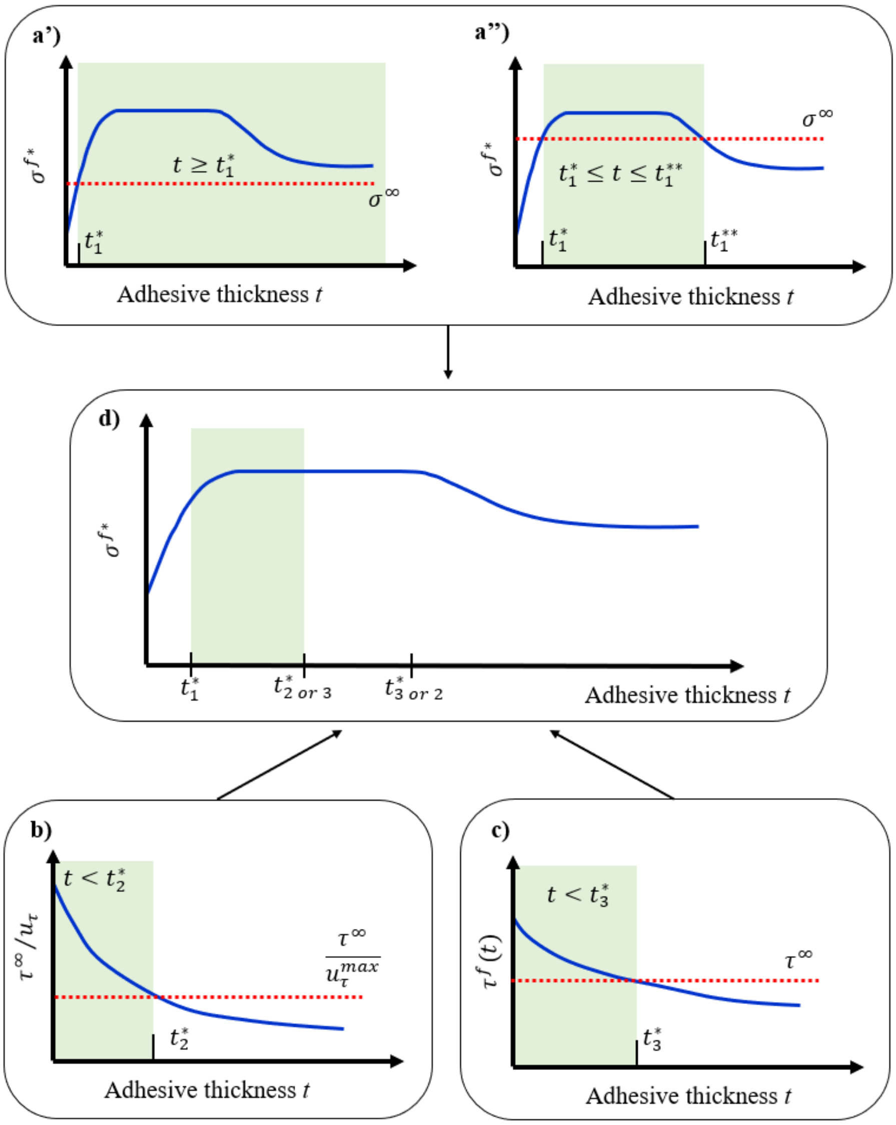
a')
σ^{f*}
$t \geq t_1^*$
σ^∞
t_1^*
Adhesive thickness t
a'')
σ^{f*}
σ^∞
$t_1^* \leq t \leq t_1^{**}$
t_1^*
t_1^{**}
Adhesive thickness t
d)
σ^{f*}
t_1^*
$t_{2\ or\ 3}^*$
$t_{3\ or\ 2}^*$
Adhesive thickness t
b)
τ^∞/u_τ
$t < t_2^*$
$\frac{\tau^\infty}{u_\tau^{max}}$
t_2^*
Adhesive thickness t
c)
$\tau^f(t)$
$t < t_3^*$
τ^∞
t_3^*
Adhesive thickness t

Figure 4

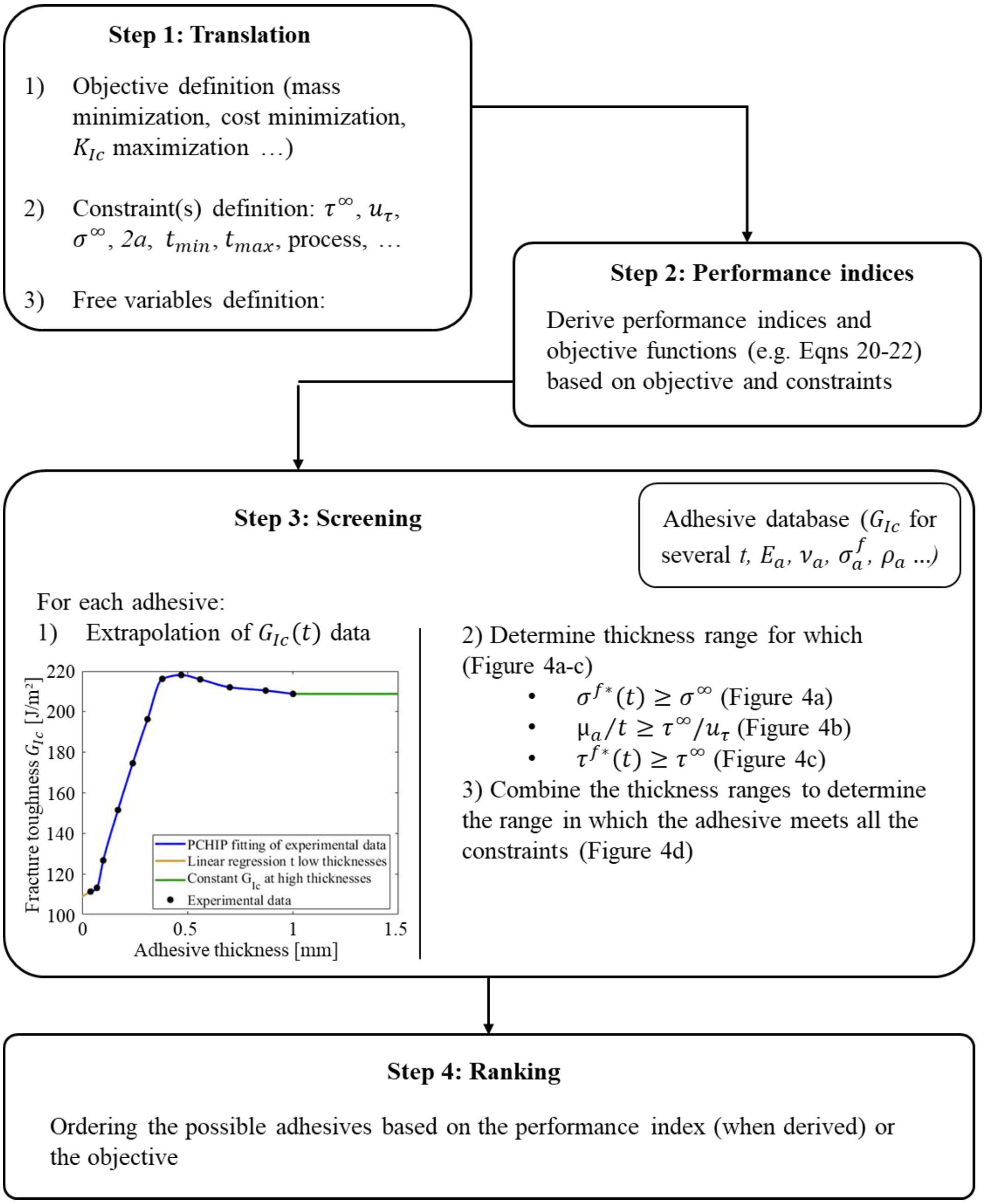
Step 1: Translation
1) Objective definition (mass minimization, cost minimization, K_{Ic} maximization …)
2) Constraint(s) definition: τ^{∞}, u_{τ}, σ^{∞}, $2a$, t_{min}, t_{max}, process, …
3) Free variables definition:
Step 2: Performance indices
Derive performance indices and objective functions (e.g. Eqns 20-22) based on objective and constraints
Step 3: Screening
Adhesive database (G_{Ic} for several t, E_a, ν_a, σ_a^f, ρ_a ...)
For each adhesive:
1) Extrapolation of $G_{Ic}(t)$ data
Fracture toughness G_{Ic} [J/m²]
Adhesive thickness [mm]
PCHIP fitting of experimental data
Linear regression t low thicknesses
Constant G_{Ic} at high thicknesses
Experimental data
2) Determine thickness range for which (Figure 4a-c)
$\sigma^{f*}(t) \geq \sigma^{\infty}$ (Figure 4a)
$\mu_a/t \geq \tau^{\infty}/u_{\tau}$ (Figure 4b)
$\tau^{f*}(t) \geq \tau^{\infty}$ (Figure 4c)
3) Combine the thickness ranges to determine the range in which the adhesive meets all the constraints (Figure 4d)
Step 4: Ranking
Ordering the possible adhesives based on the performance index (when derived) or the objective

Figure 5

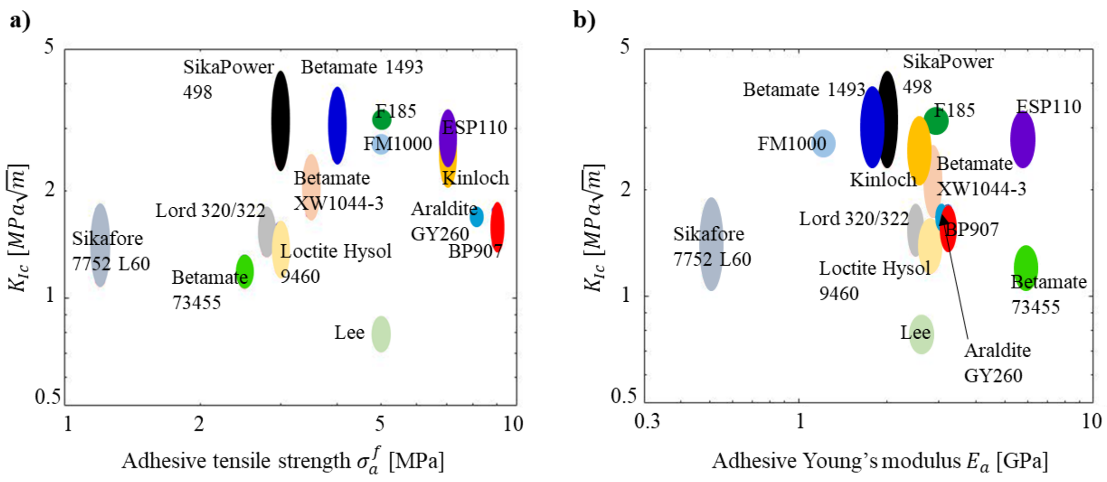
a)
b)
SikaPower 498
Betamate 1493
F185
ESP110
FM1000
Kinloch
Betamate XW1044-3
Lord 320/322
Araldite GY260
Sikafore 7752 L60
Loctite Hysol 9460
BP907
Betamate 73455
Lee
K_{Ic} $[MPa\sqrt{m}]$
Adhesive tensile strength σ_a^f [MPa]
Adhesive Young's modulus E_a [GPa]

Figure 6

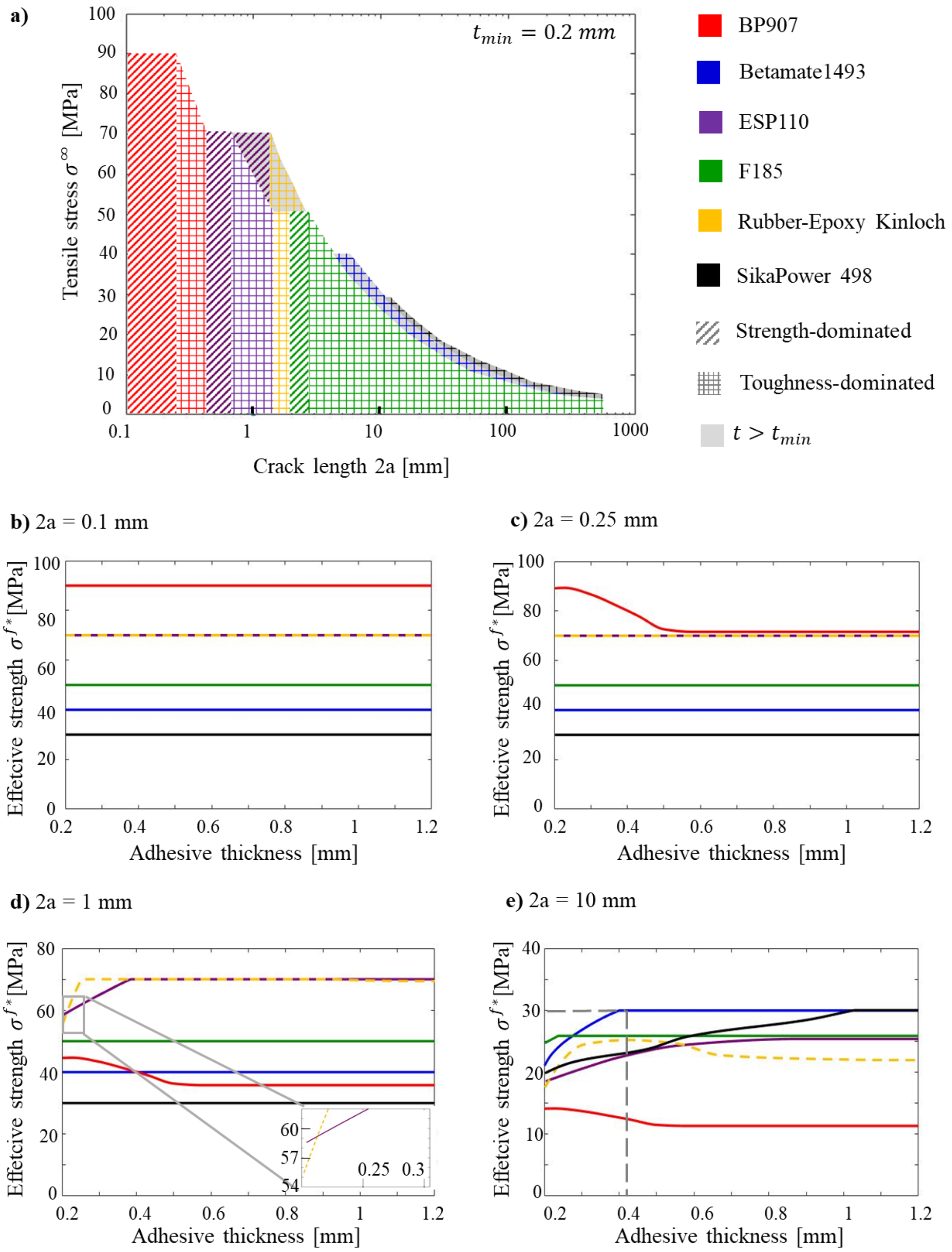

a)
$t_{min} = 0.2\ mm$
Tensile stress σ^∞ [MPa]
Crack length 2a [mm]
BP907
Betamate1493
ESP110
F185
Rubber-Epoxy Kinloch
SikaPower 498
Strength-dominated
Toughness-dominated
$t > t_{min}$
b) 2a = 0.1 mm
c) 2a = 0.25 mm
d) 2a = 1 mm
e) 2a = 10 mm
Effetcive strength σ^{f*}[MPa]
Adhesive thickness [mm]

Figure 7

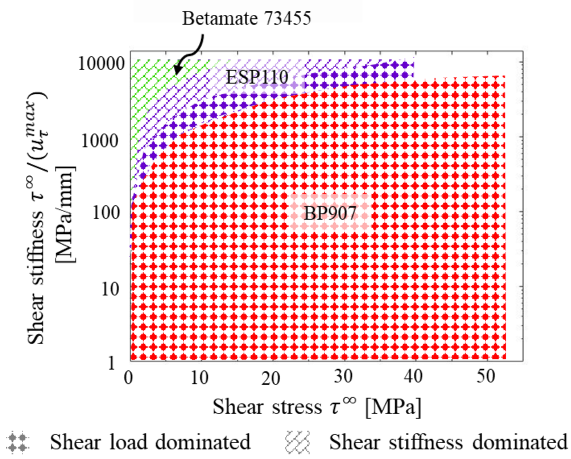
Betamate 73455
ESP110
BP907
10000
1000
100
10
1
0
10
20
30
40
50
Shear stiffness $\tau^{\infty}/(u_{\tau}^{max})$ [MPa/mm]
Shear stress τ^{∞} [MPa]
Shear load dominated
Shear stiffness dominated

Figure 8

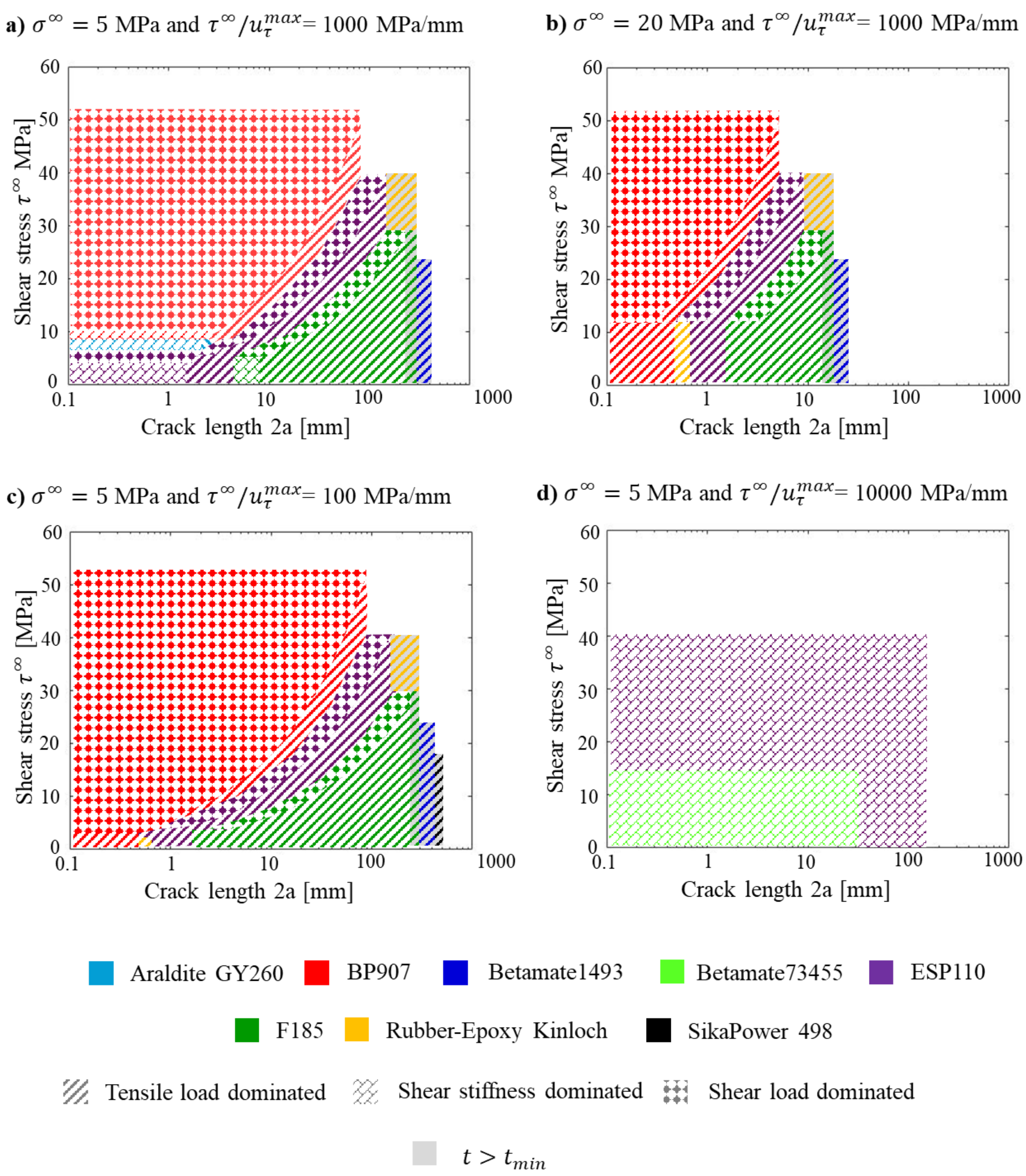
a) σ^∞ = 5 MPa and τ^∞/u_τ^{max}= 1000 MPa/mm
b) σ^∞ = 20 MPa and τ^∞/u_τ^{max}= 1000 MPa/mm
c) σ^∞ = 5 MPa and τ^∞/u_τ^{max}= 100 MPa/mm
d) σ^∞ = 5 MPa and τ^∞/u_τ^{max}= 10000 MPa/mm
Shear stress τ^∞ [MPa]
Crack length 2a [mm]
0
10
20
30
40
50
60
0.1
1
10
100
1000
Araldite GY260
BP907
Betamate1493
Betamate73455
ESP110
F185
Rubber-Epoxy Kinloch
SikaPower 498
Tensile load dominated
Shear stiffness dominated
Shear load dominated
$t > t_{min}$

Figure 9

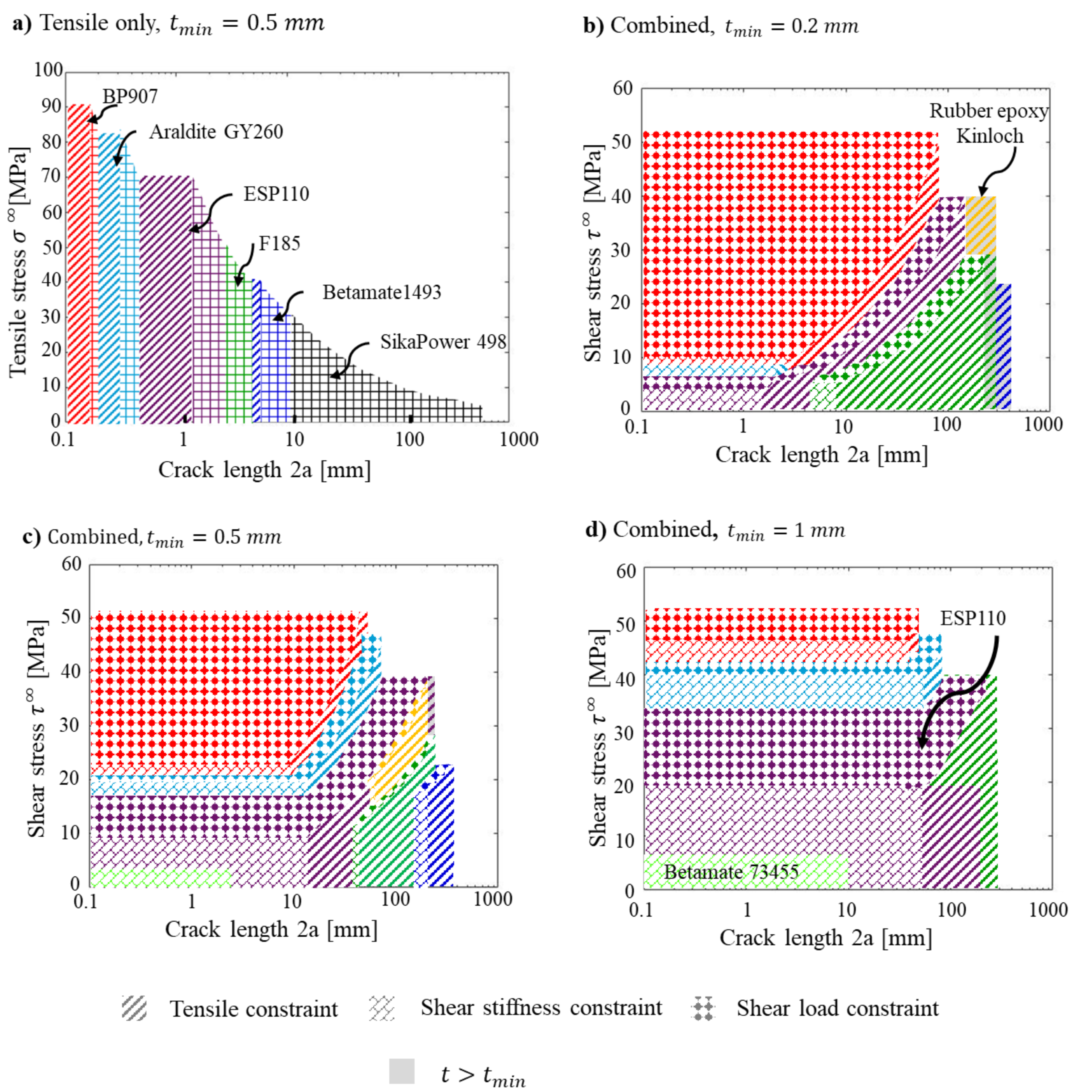

a) Tensile only, $t_{min} = 0.5\ mm$
Tensile stress σ^{∞}[MPa]
BP907
Araldite GY260
ESP110
F185
Betamate1493
SikaPower 498
Crack length 2a [mm]
b) Combined, $t_{min} = 0.2\ mm$
Shear stress τ^{∞} [MPa]
Rubber epoxy
Kinloch
Crack length 2a [mm]
c) Combined, $t_{min} = 0.5\ mm$
Shear stress τ^{∞} [MPa]
Crack length 2a [mm]
d) Combined, $t_{min} = 1\ mm$
Shear stress τ^{∞} [MPa]
ESP110
Betamate 73455
Crack length 2a [mm]
Tensile constraint
Shear stiffness constraint
Shear load constraint
$t > t_{min}$

Figure 10

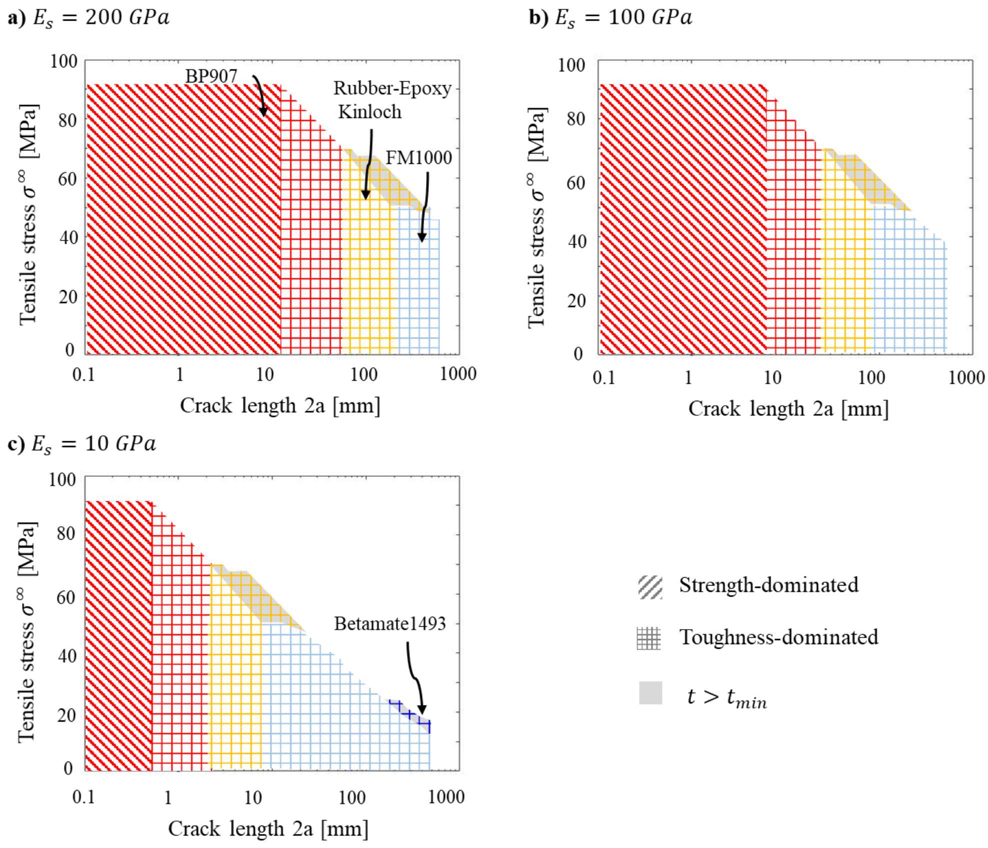

Figure 11

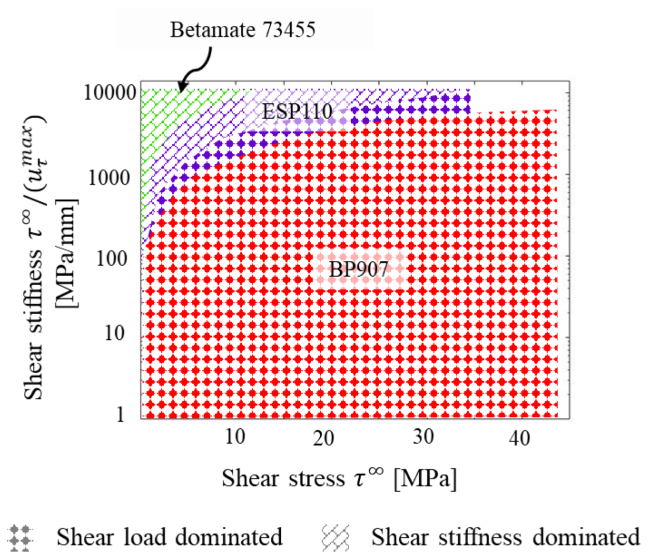

Figure 12

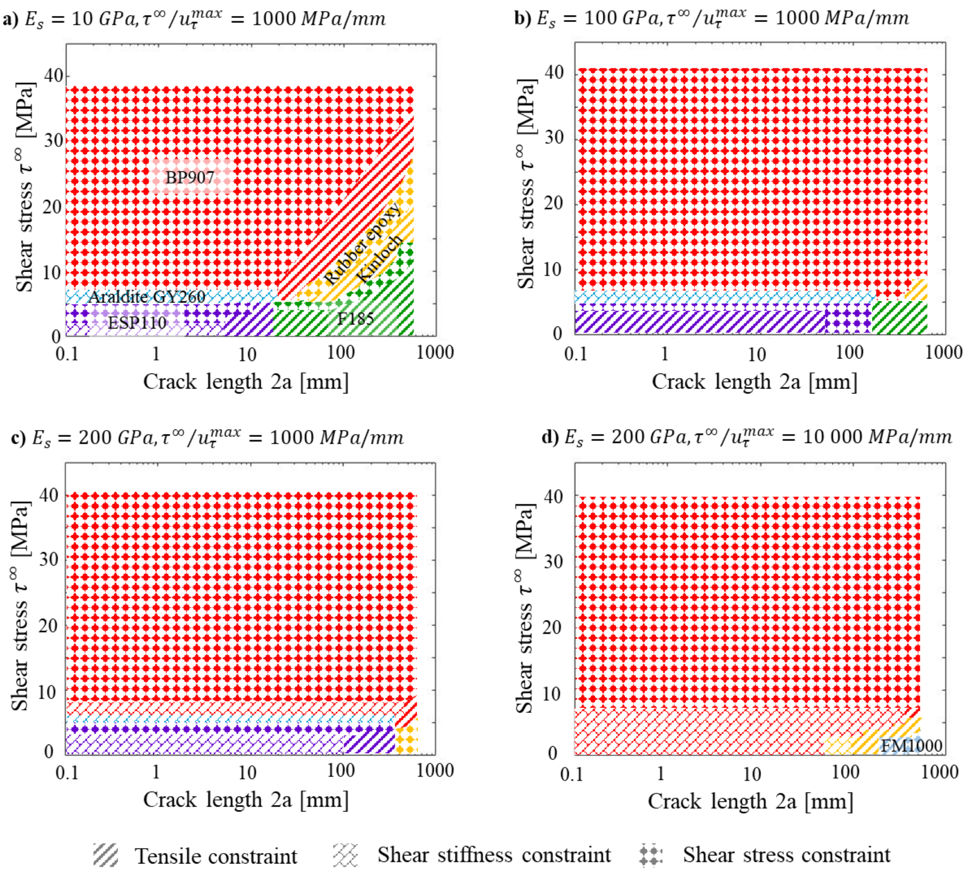

Figure 13

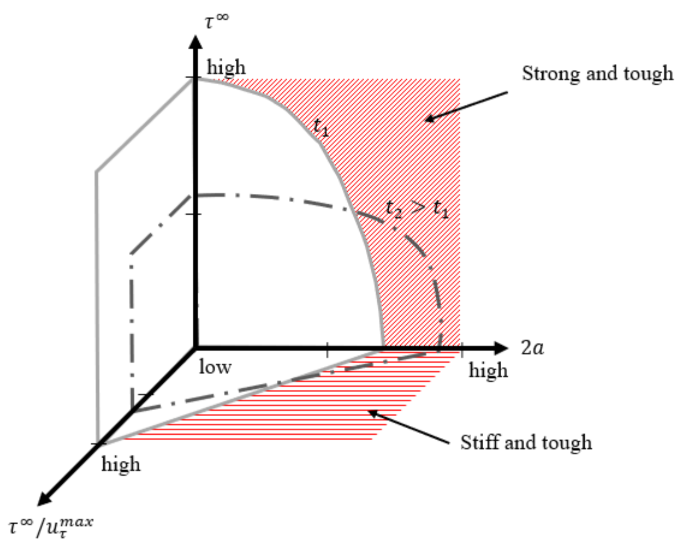

Figure 14

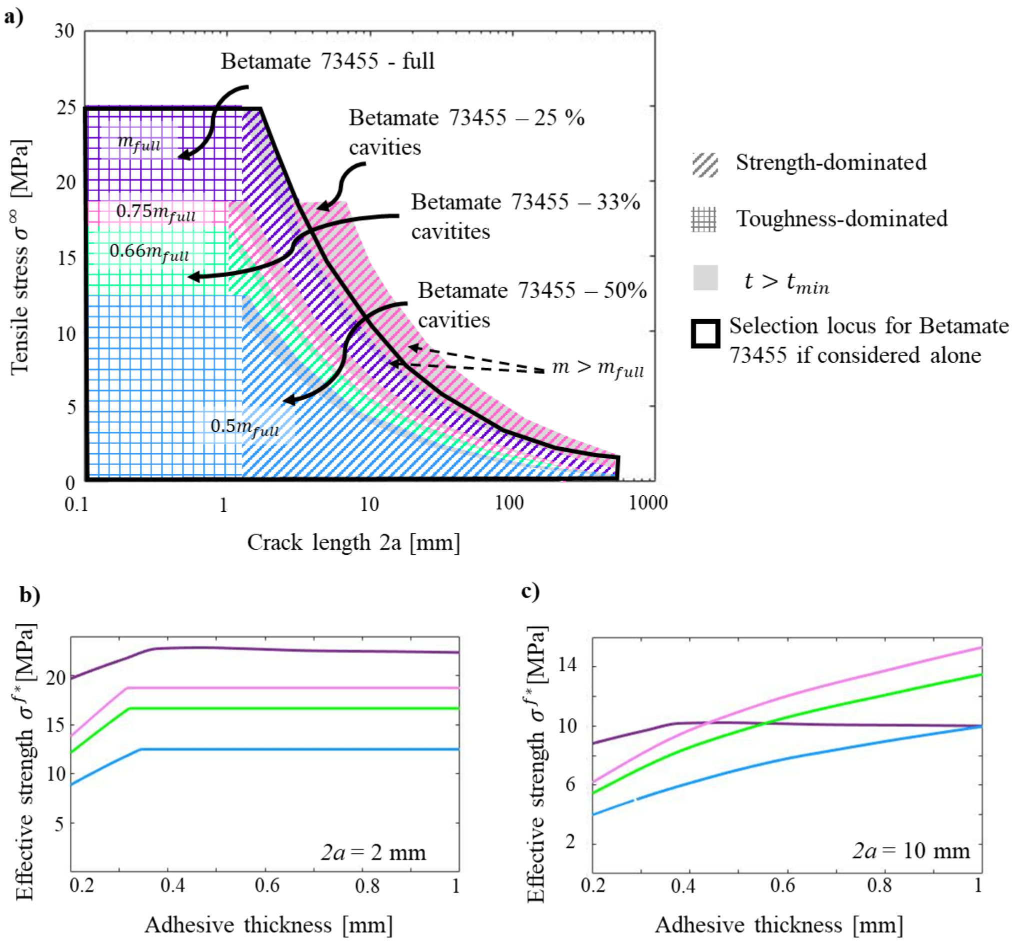

Figure 15

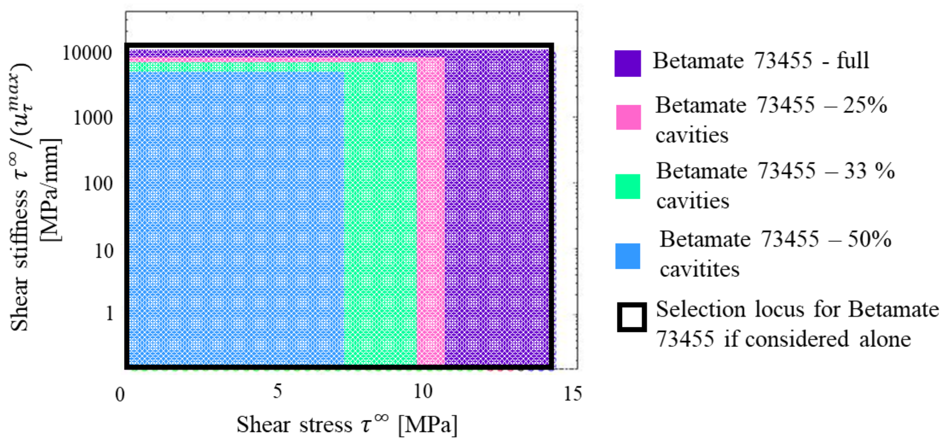

Figure 16

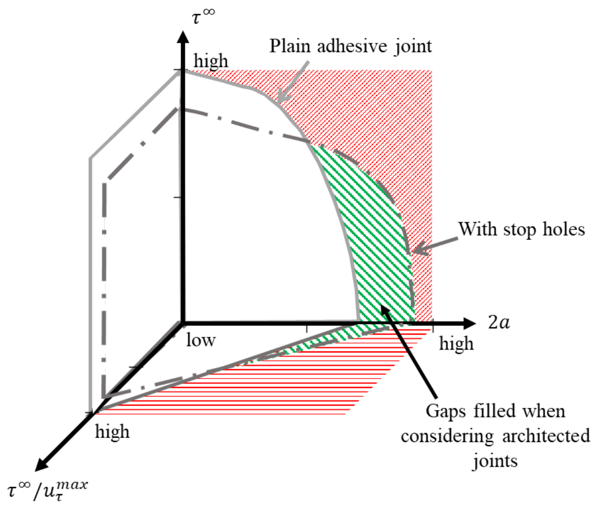

Figure 17

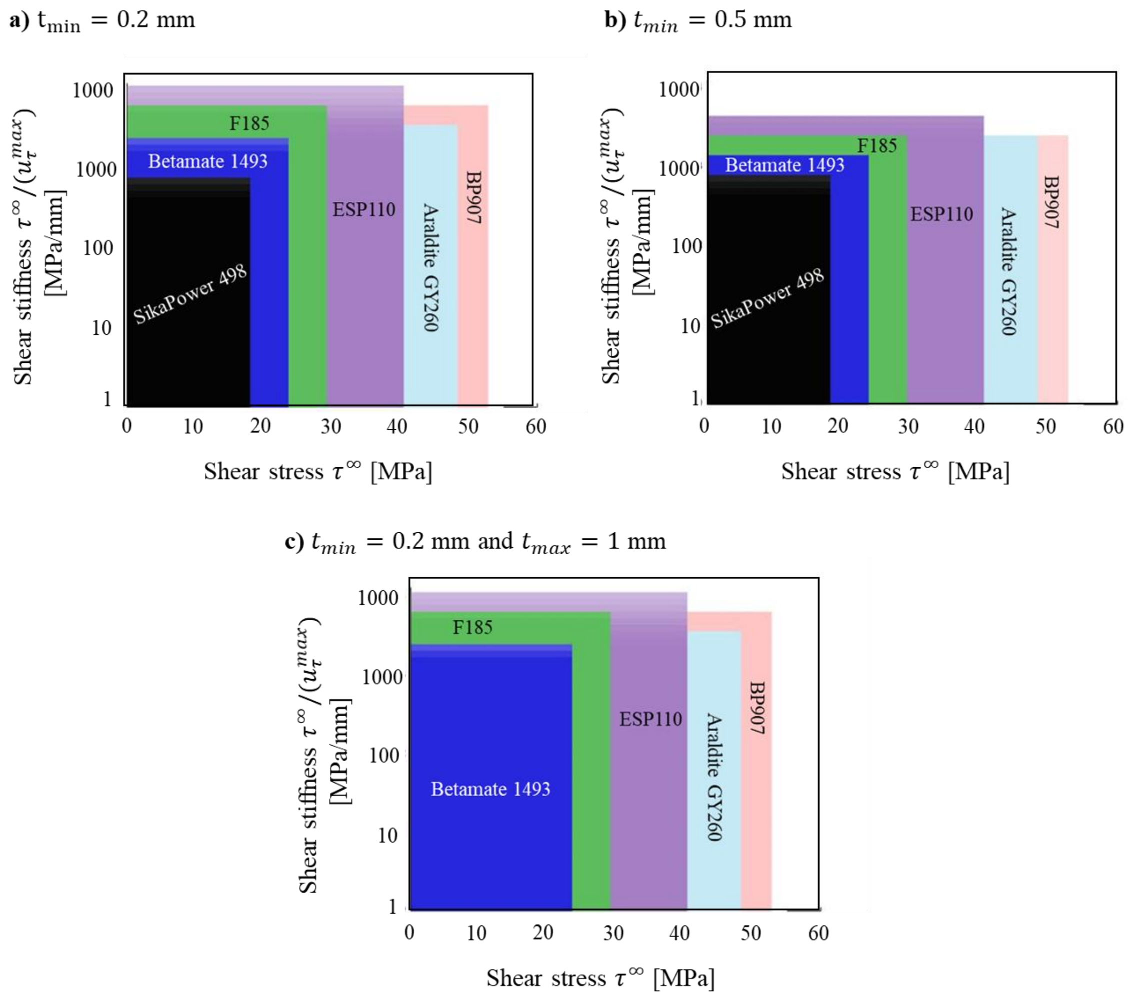

Figure C.1

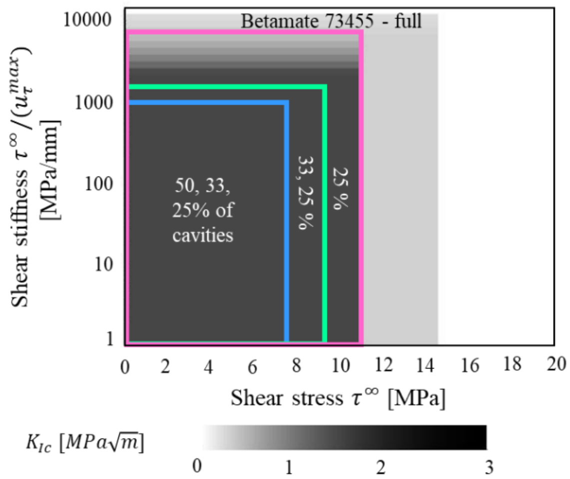

Figure C.2

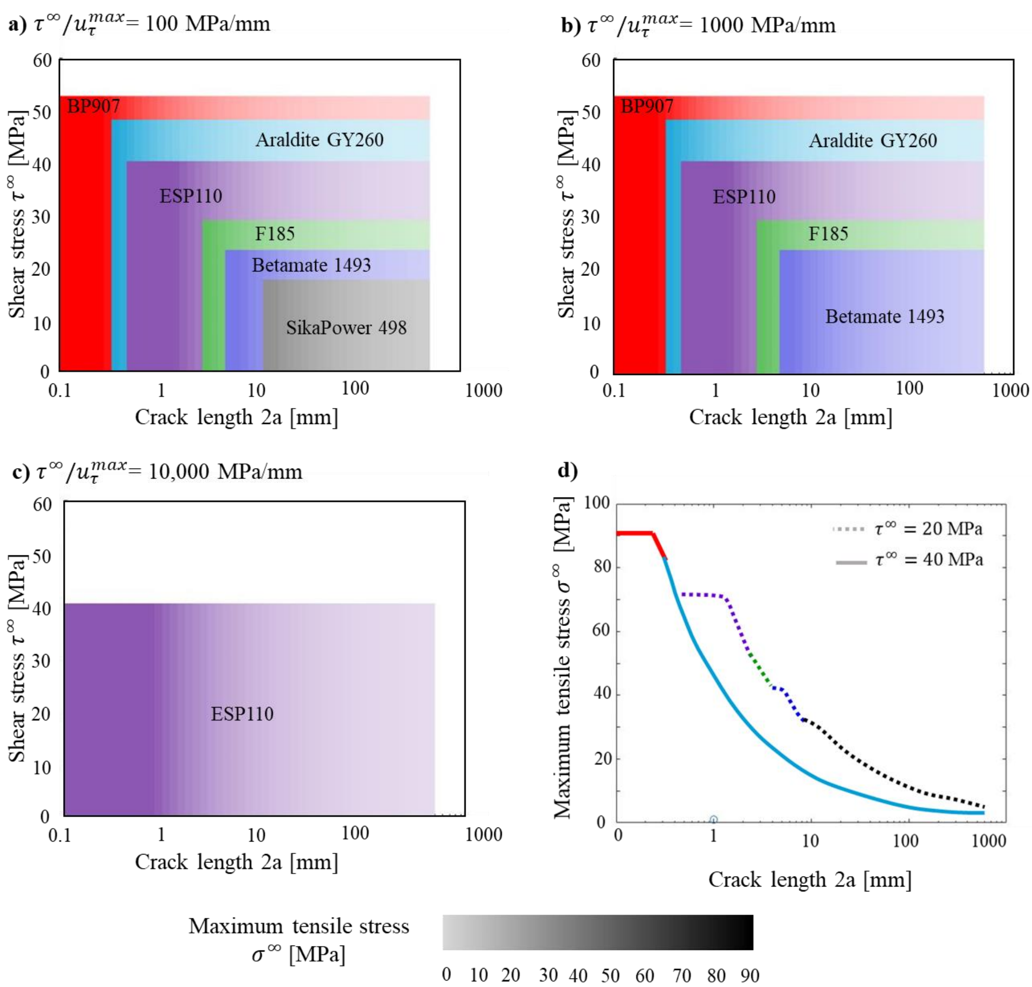

Figure D.1

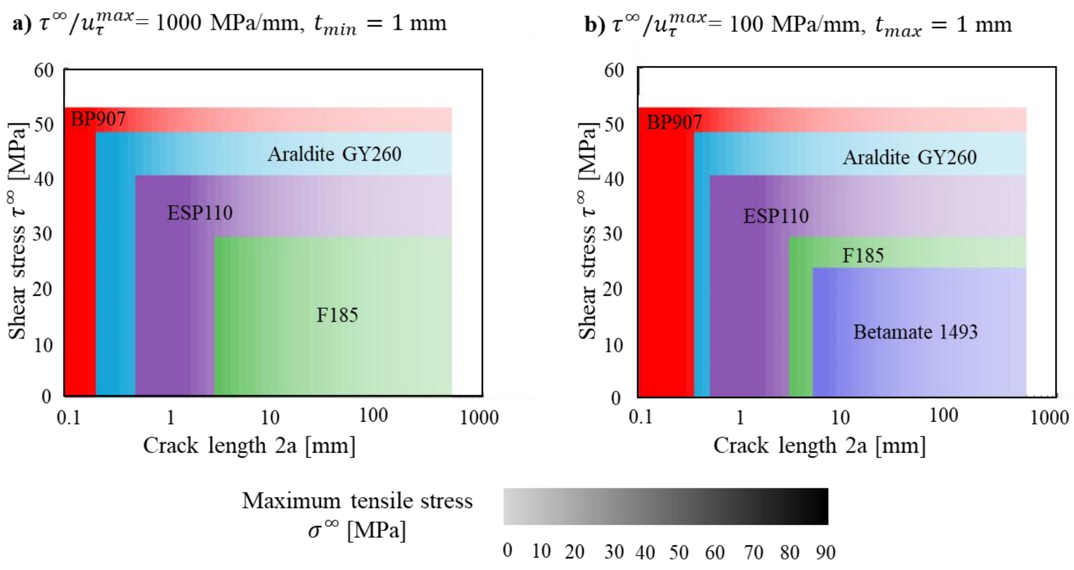

Figure D.2

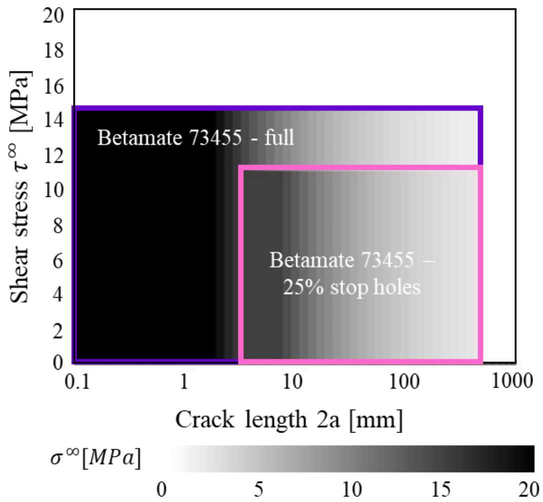

Figure D.3

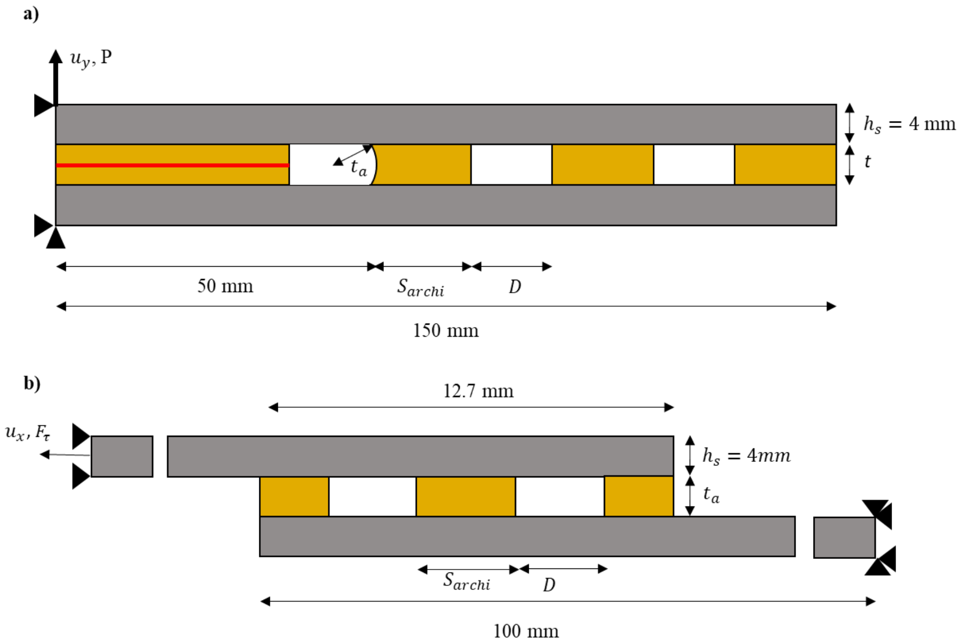

Figure E.1

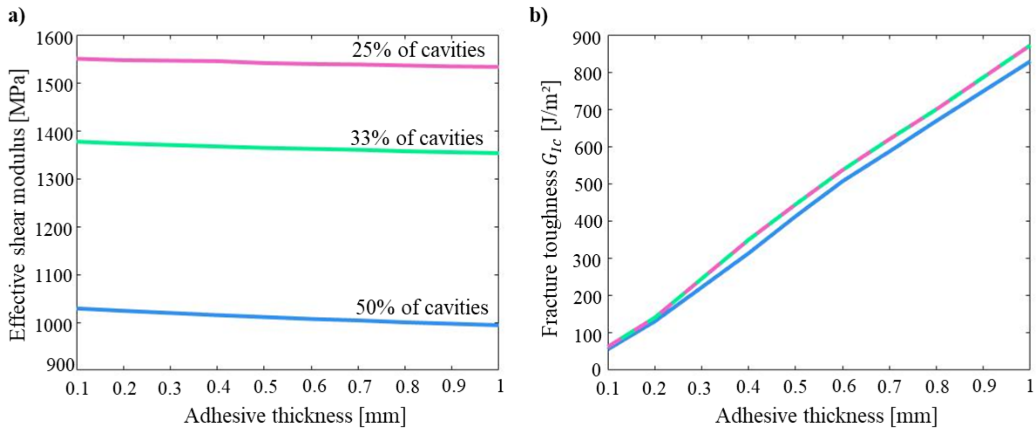

Figure E.2

Figure 1: Impact of thickness on adhesive joint properties: a) fracture toughness (adhesive of type A (blue curve) and type B (red curve)); b) tensile and shear stress distribution in tensile butt tests close to interface; c) peel and shear stress distribution in lap shear joints close to interface (results from FE simulations with the software Abaqus, based on an elastoplastic adhesive behavior).

Figure 2: Schematic of the adhesive joint with its dimensions: width W, bonded length L_a, adherend lengths L_{s1} and L_{s2}, thickness of the adherends h_s and of the adhesive t. A crack of length 2a is present in the joint subjected to both tensile and shear loads.

Figure 3: Failure regime maps of joints subjected to tensile stresses, based on Van Loock et al.[36]*.The transition between regimes A, B, C and D are shown for mismatch ratios E_a/E_s from 1 to 0.001. A and B are controlled by the adhesives only with A being the strength-controlled regime and B the toughness-controlled one. C and D are the two regimes for which the adherends have an influence with C being the toughness-controlled regime and D the strength-controlled regime.*

Figure 4: Determination of the admissible thickness range for a given adhesive from a) the tensile constraint when the constraint gives a') a lower bound or a'') a lower and an upper bound; b) the shear stiffness constraint and c) the shear strength constraint. d) is the combination of the possible thickness ranges reported on a graph giving the maximum tensile stress that can be applied to the joint depending on the adhesive thickness.

Figure 5: Graphical workflow of the selection process: step 1 translation into objective and constraints, step 2 derivation of the performance indices, step 3 screening of the database with the extrapolation of the experimental data and determining the thickness range for which each adhesive meets the constraints and step 4 ranking of the adhesive based on the objective and performance indices.

Figure 6: Ashby maps for the adhesives of the database a) $K_{Ic}(t \geq 0.2\ mm)$ versus adhesive tensile strength and b) $K_{Ic}(t \geq 0.2\ mm)$ versus adhesives Young's modulus.

Figure 7: a) Constraint chart for light adhesive joints for different applied tensile stress σ^{∞} and crack length 2a without shear loading. b)-d) Evolution of the apparent tensile strength of the adhesives with the thickness for several crack lengths b) 0.1 mm; c) 0.25 mm; d) 1 mm and e) 10 mm.

Figure 8: Influence of the shear stiffness and the applied shear stress on the adhesive selection for $t_{min} = 0.2$ mm.

Figure 9: Investigation of the combined effect of tensile and shear loading on the choice of best light adhesive for different remote tensile stress σ^{∞} and imposed shear stiffness: a) $\sigma^{\infty} = 5$ MPa and $\tau^{\infty}/u_{\tau}^{max}$ = 1000 MPa/mm; b) $\sigma^{\infty} = 20$ MPa and $\tau^{\infty}/u_{\tau}^{max}$ = 1000 MPa/mm; c) $\sigma^{\infty} = 5$ MPa and $\tau^{\infty}/u_{\tau}^{max}$ = 100 MPa/mm and d) $\sigma^{\infty} = 5$ MPa and $\tau^{\infty}/u_{\tau}^{max}$ = 10000 MPa/mm.

Figure 10: Influence of the imposed minimum thickness on the selection of best light adhesive for a) constraint on the tensile load only with $t_{min} = 0.5$ mm, and b) to d) for a combination of tensile load (5 MPa), shear stiffness ($1000\ MPa/mm$) and varying shear loads and crack length with t_{min} equal to b) 0.2 mm; c) 0.5 mm and d) 1 mm.

Figure 11: Adhesive selection maps when considering the tensile constraint only and the effects of the adherends with Young's modulus of a) 200 GPa, b) 100 GPa and c) 10 GPa for $t_{min} = 0.2$ mm.

Figure 12: Adhesive selection maps when considering the shear stiffness and strength constraints only and the interactions with the adherends if E_s equal 200 GPa and if t_{min} equals 0.2 mm.

Figure 13: Investigation of the combined effect of tensile and shear loading on the choice of best light adhesive for different adherends Young's modulus if the remote tensile stress is set to $\sigma^{\infty} = 5\ MPa$ and the shear stiffness to a)-c) 1000 MPa/mm or d) 10 000 MPa/mm: a) $E_s = 10\ GPa$, (b) $E_s = 100\ GPa$ and c)-d) $E_s = 200\ GPa$.

Figure 14: Schematic of the gaps in a constraint-based charts and influence of the thickness.

Figure 15: Influence of the remote tensile stress σ^{∞} and the crack length 2a on the selection of the lightest adhesive without shear loading. The joints are made of Betamate 73455, but contain 0%, 25%, 33% and 50% of stop holes. t_{min} is set to 0.2 mm.

Figure 16: Influence of the shear stiffness and the applied shear stress on the selection of light adhesive for joints made of Betamate 73455 made of 0%, 25%, 33% and 50 % of stop holes. t_{min} is set to 0.2 mm.

Figure 17: Influence of bondline architecturing with stop holes on the joint properties.

Figure C.1: Selection map for the maximization of K_{Ic} depending on the constraints on shear stiffness and shear strength for a) $t_{min} = 0.2$ mm, b) $t_{min} = 0.5$ mm and c) $t_{min} = 0.2$ mm and $t_{max} = 1$ mm.

Figure C.2.: Selection map for architected joints with stop holes when the objective is to maximize the fracture toughness.

Figure D.1: Selection map for σ^{∞} maximization depending on the crack length and the shear strength constraint for shear stiffnesses of a) 100 MPa/mm, b) 1000 MPa/mm and c) 10000 MPa/mm. d) Cuts in a) for τ^{∞} equal to 20 and 40 MPa to show the variation of σ^{∞} maximum with crack length.

Figure D.2: Selection for σ^{∞} maximization depending on the shear strength constraint and the crack length and depending on t_{min} and t_{max} with a) a stiffness of 1000 MPa/mm, $t_{min} = 1$ mm and no limit on t_{max} and with b) a stiffness of 100 MPa/mm, $t_{min} = 0.2$ mm and $t_{max} = 1$ mm.

Figure D.3: Selection map for architected joints containing stop holes when maximizing the remote tensile force and for a shear stiffness not exceeding 4000 MPa/mm.

Figure E.1: Finite element model for a) Double Cantilever Beam samples and b) Lap shear joint for architected joints with stop holes.

Figure E.2: FE simulations results for architected joints containing 25%, 33% and 50% of cavities: evolution of a) the effective shear modulus and b) the fracture toughness G_{Ic} with the adhesive thickness.